Supporting Information

Effect of fluorine atoms in flexible chains on the phase transitions and photophysical behavior of D-π-A-type 4-alkoxy-4´-cyanodiphenylacetylene

Shigeyuki Yamada,*[a] Keigo Yoshida,[a] Tsuneaki Sakurai,[a] Mitsuo Hara,[b] Tsutomu Konno[a]

[a] Faculty of Molecular Chemistry and Engineering, Kyoto Institute of Technology, Matsugasaki, Sakyo-ku, Kyoto 606-8585, Japan
[b] Department of Molecular and Macromolecular Chemistry, Graduate School of Engineering, Nagoya University, Furo-cho, Chikusa-ku, Nagoya, Aichi 464-8603, Japan

*Corresponding author.
E-mail: syamada@kit.ac.jp

Table of contents

Experimental ••••••••••••••••••••••••••••••• S-2
NMR spectra ••••••••••••••••••••••••••••••• S-7
Theoretical calculation ••••••••••••••••••••••••••••••• S-17
Cartesian coordinate ••••••••••••••••••••••••••••••• S-20
Phase transition behavior ••••••••••••••••••••••••••••••• S-23
Photophysical behavior S-27
In various solvent for **1a** ••••••••••••••••••••••••••••••• S-28
In various solvent for **1b** ••••••••••••••••••••••••••••••• S-30
In various solvent for **1c** ••••••••••••••••••••••••••••••• S-32
In crystalline phase ••••••••••••••••••••••••••••••• S-34
Powder XRD pattern of **1a**–**c**••••••••••••••••••••••••••••••• S-35
In LC phase ••••••••••••••••••••••••••••••• S-36

Experimental

General

All reactions were carried out using dried glassware with a magnetic stirrer bar. All chemicals were of reagent grade and where necessary were purified in the usual manner prior to use. Column chromatography was carried out on silica gel (Wakogel® 60N, 38–100 μm), and thin-layer chromatography (TLC) analysis was performed on silica gel TLC plates (Merck, silica gel $60F_{254}$). ^{1}H and ^{13}C NMR spectra were obtained using a Bruker AVANCE III 400 NMR spectrometer (^{1}H: 400 MHz and ^{13}C: 100 MHz) in chloroform-*d* ($CDCl_3$) solution, and the chemical shifts are reported in parts per million (ppm) using the residual proton in the NMR solvent. ^{19}F NMR (376 MHz) spectra were also obtained with a Bruker AVANCE III 400 NMR spectrometer in $CDCl_3$ with hexafluorobenzene (C_6F_6, $\delta_F = -163$ ppm) as an internal standard. Infrared (IR) spectra were acquired using the KBr method and a JASCO FT/IR-4100 type A spectrometer; all spectra were reported in wavenumbers (cm^{-1}). High resolution mass spectra (HRMS) were recorded using a JEOL JMS-700MS spectrometer and the fast atom bombardment (FAB) method. Melting temperature (T_m) and clearing temperature (T_c) were determined from onset values obtained via differential scanning calorimetry.

*Preparation of **2a** from 4-bromo-1-decyloxybenzene*

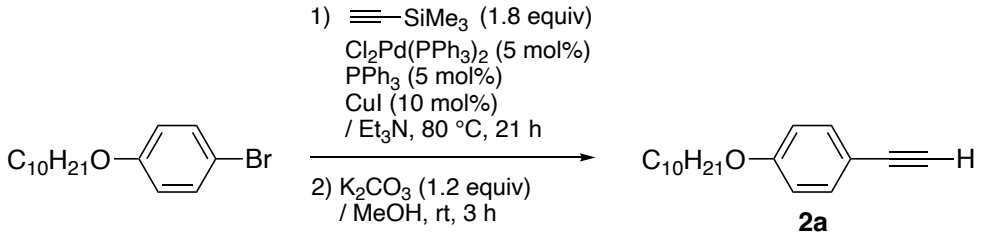

In a two-necked round-bottomed flask, equipped with a Teflon®-coated stirring bar, was placed 4-bromo-1-decyloxybenzene (7.24 g, 28.2 mmol), $Cl_2Pd(PPh_3)_2$ (1.01 g, 1.48 mmol), PPh_3 (0.76 g, 1.48 mmol), and Et_3N (100 mL). To the solution was added CuI (0.31 g, 2.96 mmol) and trimethylsilylacetylene (4.96 g, 50.5 mmol), and the solution was stirred at 80 °C for 21 h. After being stirred for 21 h, precipitate formed during the reaction was separated by atmospheric filtration, and the filtrate was poured into saturated aqueous NH_4Cl solution. The crude product was extracted with Et_2O (50 mL) three times. The combined organic layer was dried over anhydrous sodium sulfate (Na_2SO_4), filtered under atmospheric pressure, and evaporated under reduced pressure using a rotary evaporator. After flash column chromatography using hexane/EtOAc 40/1 (v/v) mixed solvent as an eluent, the corresponding coupling product was obtained in 40% (3.04 g, 11.1 mmol) as yellow oil, which was used for the following reaction without further purification; In a round-bottomed flask was placed the above prepared TMS-terminated phenylacetylene (3.04 g, 11.1 mmol) and potassium carbonate (1.84 g, 13.3 mmol), and MeOH (55 mL). The whole was stirred at room temperature for 3 h. The resultant solution was poured into aqueous NH_4Cl solution. The crude product was extracted with Et_2O (50 mL) three times. The combined organic layer was dried over anhydrous sodium sulfate (Na_2SO_4), filtered under atmospheric pressure, and evaporated under reduced pressure using a rotary evaporator. The residue was subjected to silica-gel column chromatography using hexane/EtOAc 40/1 (v/v) mixed solvent as an eluent, producing the precursor **2a** in 53% (1.09 g, 5.9 mmol) as a white solid.

4-Decyloxyphenylacetylene (2a)

Yield: 53% (white solid); ^{1}H NMR ($CDCl_3$): δ 0.89 (t, J = 7.2 Hz, 3H), 1.22–1.39 (m, 12H), 1.45 (quin, J = 7.6 Hz, 2H), 1.78 (quin, J = 8.0 Hz, 2H), 2.99 (s, 1H), 3.95 (t, J = 6.4 Hz, 2H), 6.83 (d, J = 8.8 Hz, 2H), 7.42 (d, J = 8.8 Hz, 2H); ^{13}C NMR ($CDCl_3$): δ 14.1, 22.6, 26.0, 29.1, 29.3, 29.4, 29.6, 31.9, 67.9, 75.6, 83.7, 113.8, 114.3, 133.4, 159.4 (one alkyl peak was overlapped with other peaks.); All physical data are fully in accordance with reported ones.[1]

*Synthesis of **1a** via Sonogashira cross-coupling reaction of 4-bromobenzonitrile with 4-decyloxyphenylacetylene*

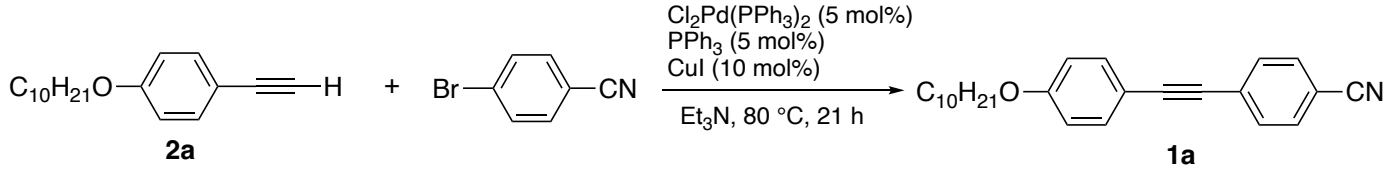

In a two-necked round-bottomed flask, equipped with a Teflon®-coated stirring bar, was placed 4-bromobenzonitrile (1.00 g, 5.5 mmol), $Cl_2Pd(PPh_3)_2$ (0.19 g, 0.28 mmol), PPh_3 (0.072 g, 0.28 mmol), and Et_3N (35 mL). To the solution was added CuI (0.105 g, 0.56 mmol) and 4-decyloxyphenylacetylene (2.58 g, 10 mmol), and the solution was stirred at 80 °C for 21 h. After being stirred for 21 h, precipitate formed during the reaction was separated by atmospheric filtration, and the filtrate was poured into saturated aqueous NH_4Cl solution. The crude product was extracted with Et_2O (50 mL) three times. The combined organic layer was dried over anhydrous sodium sulfate (Na_2SO_4), filtered under atmospheric pressure, and evaporated under reduced pressure using a rotary evaporator. The residue was subjected to silica-gel column chromatography using hexane/EtOAc 20/1 (v/v) mixed solvent as an eluent, followed by recrystallization from CH_2Cl_2/methanol (v/v = 1/1), producing the coupling product **1a** in 56% (1.11 g, 3.1 mmol) as a white solid.

4-Decyloxy-4'-cyanodiphenylacetylene (1a)

Yield: 56% (white solid); M.p.: T_m = 63 °C, T_c = 92 °C (cooling process); ^{1}H NMR ($CDCl_3$): δ 0.89 (t, J = 7.2 Hz, 3H), 1.22–1.40 (m, 12H), 1.40–1.52 (m, 2H), 1.79 (quin, J = 8.0 Hz, 2H), 3.97 (t, J = 6.4 Hz, 2H), 6.88 (d, J = 8.8 Hz, 2H), 7.46 (d, J = 8.8 Hz, 2H), 7.57 (d, J = 8.4 Hz, 2H), 7.61 (d, J = 8.4 Hz, 2H); ^{13}C NMR ($CDCl_3$): δ 14.1, 22.6, 26.0, 29.1, 29.29, 29.34, 29.5, 31.9, 68.1, 86.6, 94.2, 110.9, 113.9, 114.6, 118.6, 128.7, 131.8, 132.0, 133.3, 159.9 (one alkyl peak was overlapped with other peaks.); IR (KBr): ν 3039, 2954, 2870, 2236, 2211, 1569, 1305, 1270, 1024, 836 cm^{-1}; HRMS (FAB) Calcd for (M^+) $C_{25}H_{29}NO$: 359.2249, Found: 359.2244.

*Preparation of **2b** from 4-bromo-1-(7,7,8,8,9,9,10,10,10-nonafluorodecyloxy)benzene*

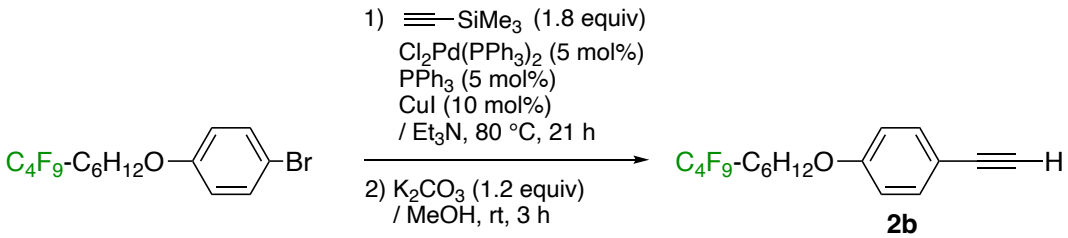

In a two-necked round-bottomed flask, equipped with a Teflon®-coated stirring bar, was placed 4-bromo-1-(7,7,8,8,9,9,10,10,10-nonafluorodecyloxy)benzene (4.81 g, 10.2 mmol), $Cl_2Pd(PPh_3)_2$ (0.35 g, 0.51 mmol), PPh_3 (0.13 g, 0.51 mmol), and Et_3N (36 mL). To the solution was added CuI (0.19 g, 1.02 mmol) and

[1] J.D. Wood, J.L. Jellison, A.D. Finke, L. Wang, L.N. Plunkett, *J. Am. Chem. Soc.* **2012**, *38*, 15783.

trimethylsilylacetylene (1.76 g, 18.4 mmol), and the solution was stirred at 80 °C for 21 h. After being stirred for 21 h, precipitate formed during the reaction was separated by atmospheric filtration, and the filtrate was poured into saturated aqueous NH_4Cl solution. The crude product was extracted with Et_2O (50 mL) three times. The combined organic layer was dried over anhydrous sodium sulfate (Na_2SO_4), filtered under atmospheric pressure, and evaporated under reduced pressure using a rotary evaporator. After flash column chromatography using hexane/EtOAc 20/1 (v/v) mixed solvent as an eluent, the corresponding coupling product was obtained in 45% (2.24 g, 4.5 mmol) as yellow oil, which was used for the following reaction without further purification; In a round-bottomed flask was placed the above prepared TMS-terminated phenylacetylene (2.24 g, 4.5 mmol) and potassium carbonate (0.75 g, 5.4 mmol), and MeOH (23 mL). The whole was stirred at room temperature for 3 h. The resultant solution was poured into aqueous NH_4Cl solution. The crude product was extracted with Et_2O (50 mL) three times. The combined organic layer was dried over anhydrous sodium sulfate (Na_2SO_4), filtered under atmospheric pressure, and evaporated under reduced pressure using a rotary evaporator. The residue was subjected to silica-gel column chromatography using hexane/EtOAc 20/1 (v/v) mixed solvent as an eluent, producing 4-(7,7,8,8,9,9,10,10,10-nonafluorodecyloxy)phenylacetylene (**2b**) in 43% (0.82 g, 2.0 mmol) as a colorless oil.

4-(7,7,8,8,9,9,10,10,10-Nonafluorodecyloxy)phenylacetylene (2b)

Yield: 43% (colorless oil); ^{1}H NMR ($CDCl_3$): δ 1.40–1.58 (m, 4H), 1.65 (quin, J = 7.2 Hz, 2H), 1.80 (quin, J = 6.8 Hz, 2H), 2.01–2.16 (m, 2H), 3.00 (s, 1H), 3.96 (t, J = 6.4 Hz, 2H), 6.83 (d, J = 8.8 Hz, 2H), 7.43 (d, J = 8.8 Hz, 2H); ^{13}C NMR ($CDCl_3$): δ 20.0, 25.7, 28.8, 28.9, 30.7 (t, J = 21.9 Hz), 67.7, 75.7, 83.7, 114.1, 114.4, 133.6, 159.4 (Carbon signals for C_4F_9 moiety could not be properly identified because they were complicatedly divided by the coupling with the fluorine nucleus.); ^{19}F NMR ($CDCl_3$, C_6F_6): δ –82.31 (t, J = 9.4 Hz, 3F), –115.9 (quin, J = 16.2 Hz, 2F), –125.6 to –125.8 (m, 2F), 127.32 (t, J = 12.0 Hz, 2F); IR (neat): ν 2946, 2870, 2108, 1607, 1508, 1471, 1356, 1289, 1171, 879 cm^{-1}; HRMS (FAB) Calcd for (M^+) $C_{18}H_{17}F_9O$: 420.1136, Found: 420.1131.

*Synthesis of **1b** via Sonogashira cross-coupling reaction of 4-bromobenzonitrile with 4-decyloxyphenylacetylene*

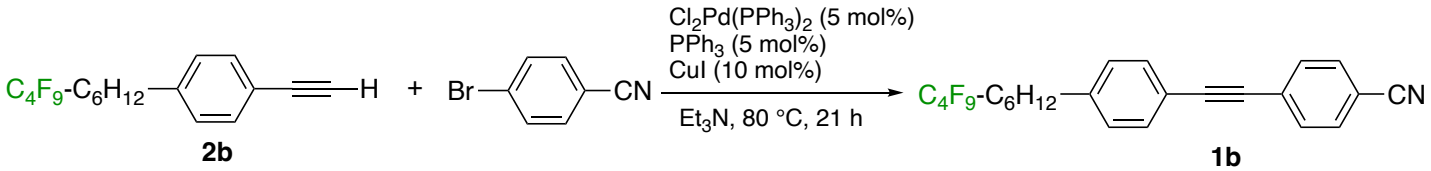

In a two-necked round-bottomed flask, equipped with a Teflon®-coated stirring bar, was placed 4-bromobenzonitrile (0.33 g, 1.8 mmol), $Cl_2Pd(PPh_3)_2$ (0.040 g, 0.050 mmol), PPh_3 (0.013 g, 0.050 mmol), and Et_3N (3.3 mL). To the solution was added CuI (0.020 g, 0.10 mmol) and 4-(7,7,8,8,9,9,10,10,10-nonafluorodecyloxy)phenylacetylene (**2b**) (0.42 g, 1.0 mmol), and the solution was stirred at 80 °C for 21 h. After being stirred for 21 h, precipitate formed during the reaction was separated by atmospheric filtration, and the filtrate was poured into saturated aqueous NH_4Cl solution. The crude product was extracted with Et_2O (20 mL) three times. The combined organic layer was dried over anhydrous sodium sulfate (Na_2SO_4), filtered under atmospheric pressure, and evaporated under reduced pressure using a rotary evaporator. The residue was subjected to silica-gel column chromatography using hexane/EtOAc 20/1 (v/v) mixed solvent as an eluent, followed by recrystallization from CH_2Cl_2/methanol (v/v = 1/1), producing the coupling product **1b** in 66% (0.34 g, 0.66 mmol) as a white solid.

4-Nonafluorodecyloxy-4'-cyanodiphenylacetylene (1b)

Yield: 66% (white solid); M.p.: T_m = 61 °C, T_c = 138 °C (cooling process); ^{1}H NMR ($CDCl_3$): δ 1.40–1.52 (m, 2H), 1.65 (quin, J = 8.0 Hz, 2H), 1.82 (quin, J = 7.6 Hz, 2H), 2.08 (tt, J = 18.0, 8.0 Hz, 2H), 3.99 (t, J = 6.4 Hz, 2H), 6.88 (d, J = 8.8 Hz, 2H), 7.47 (d, J = 8.8 Hz, 2H), 7.57 (d, J = 8.4 Hz, 2H), 7.62 (d, J = 8.4 Hz, 2H); ^{13}C NMR ($CDCl_3$): δ 20.1, 25.7, 28.8, 28.9, 30.7 (t, J = 22.7 Hz), 67.8, 86.7, 94.1, 111.0, 114.1, 114.6, 118.6, 128.7, 131.8, 132.0, 133.4, 159.8 (Carbon signals for C_4F_9 moiety could not be properly identified because they were complicatedly divided by the coupling with the fluorine nucleus.); ^{19}F NMR ($CDCl_3$, C_6F_6): δ –82.34 (t, J = 10.9 Hz, 3F), –115.8 to –116.1 (m, 2F), –125.7 to –125.9 (m, 2F), 127.3 to –127.5 (m, 2F); IR (KBr): ν 2937, 2857, 2235, 1601, 1514, 1467, 1359, 1241, 1024, 837 cm^{-1}; HRMS (FAB) Calcd for (M^+) $C_{25}H_{21}F_9NO$: 522.1479, Found: 522.1486.

*Preparation of **2c** from 4-bromo-1-(5,5,6,6,7,7,8,8,9,9,10,10,10-tridecafluorodecyloxy)benzene*

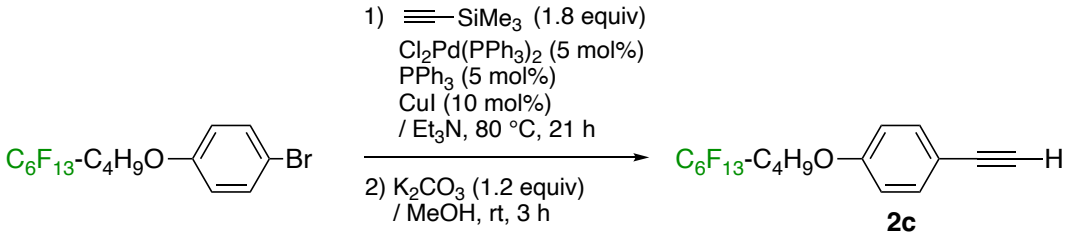

In a two-necked round-bottomed flask, equipped with a Teflon®-coated stirring bar, was placed 4-bromo-1-(5,5,6,6,7,7,8,8,9,9,10,10,10-tridecafluorodecyloxy)benzene (1.09 g, 2.0 mmol), $Cl_2Pd(PPh_3)_2$ (0.070 g, 0.10 mmol), PPh_3 (0.026 g, 0.10 mmol), and Et_3N (7.3 mL). To the solution was added CuI (0.038 g, 0.20 mmol) and trimethylsilylacetylene (0.35 g, 3.6 mmol), and the solution was stirred at 80 °C for 21 h. After being stirred for 21 h, precipitate formed during the reaction was separated by atmospheric filtration, and the filtrate was poured into saturated aqueous NH_4Cl solution. The crude product was extracted with Et_2O (50 mL) three times. The combined organic layer was dried over anhydrous sodium sulfate (Na_2SO_4), filtered under atmospheric pressure, and evaporated under reduced pressure using a rotary evaporator. After flash column chromatography using hexane/EtOAc 40/1 (v/v) mixed solvent as an eluent, the corresponding coupling product was obtained in 52% (0.59 g, 1.04 mmol) as yellow oil, which was used for the following reaction without further purification; In a round-bottomed flask was placed the above prepared TMS-terminated phenylacetylene (0.32 g, 0.56 mmol) and potassium carbonate (0.093 g, 0.67 mmol), and MeOH (2.8 mL). The whole was stirred at room temperature for 3 h. The resultant solution was poured into aqueous NH_4Cl solution. The crude product was extracted with Et_2O (10 mL) three times. The combined organic layer was dried over anhydrous sodium sulfate (Na_2SO_4), filtered under atmospheric pressure, and evaporated under reduced pressure using a rotary evaporator. The residue was subjected to silica-gel column chromatography using hexane/EtOAc 40/1 (v/v) mixed solvent as an eluent, producing 4-(5,5,6,67,7,8,8,9,9,10,10,10-tridecafluorodecyloxy)phenylacetylene (**2c**) in 82% (0.23 g, 0.46 mmol) as a colorless oil.

4-(5,5,6,67,7,8,8,9,9,10,10,10-tridecafluorodecyloxy)phenylacetylene (2c)

Yield: 82% (colorless oil); ^{1}H NMR ($CDCl_3$): δ 1.76–1.93 (m, 4H), 2.08–2.24 (m, 2H), 3.00 (s, 1H), 4.00 (t, J = 5.6 Hz, 2H), 6.83 (d, J = 8.8 Hz, 2H), 7.43 (d, J = 8.8 Hz, 2H); ^{13}C NMR ($CDCl_3$): δ 17.3, 28.6, 30.7 (t, J = 22.0 Hz), 67.2, 75.8, 83.6, 114.4, 132.3, 133.6, 159.2 (Carbon signals for C_6F_{13} moiety could not be properly identified

because they were complicatedly divided by the coupling with the fluorine nucleus.); ^{19}F NMR ($CDCl_3$, C_6F_6): δ –82.05 (t, J = 9.4 Hz, 3F), –115.74 (brs, 2F), –123.21 (brs, 2F), –124.16 (brs, 2F), –124.82 (brs, 2F), –127.43 (brs, 2F); IR (neat): ν 2927, 2884, 2108, 1606, 1507, 1472, 1242, 1038, 833 cm^{-1}; HRMS (FAB) Calcd for (M^+) $C_{18}H_{13}F_{13}O$: 492.0759, Found: 492.0758.

*Synthesis of **1c** via Sonogashira cross-coupling reaction of 4-bromobenzonitrile with 4-(5,5,6,6,7,7,8,8,9,9,10,10,10-tridecafluorodecyloxy)phenylacetylene*

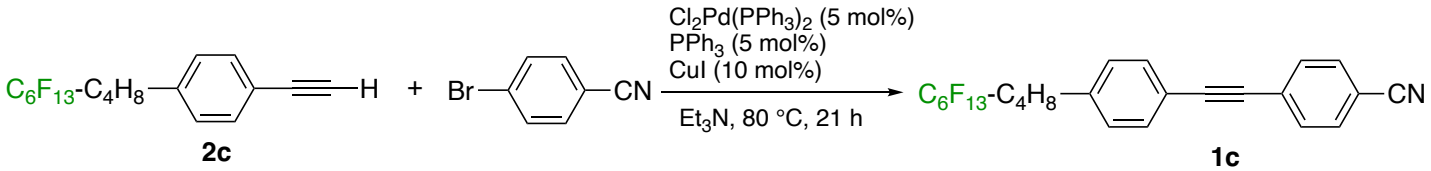

In a two-necked round-bottomed flask, equipped with a Teflon®-coated stirring bar, was placed 4-bromobenzonitrile (0.18 g, 1.0 mmol), $Cl_2Pd(PPh_3)_2$ (0.035 g, 0.050 mmol), PPh_3 (0.013 g, 0.050 mmol), and Et_3N (3.3 mL). To the solution was added CuI (0.020 g, 0.10 mmol) and 4-(5,5,6,6,7,7,8,8,9,9,10,10,10-tridecafluorodecyloxy)phenylacetylene (0.89 g, 1.8 mmol), and the solution was stirred at 80 °C for 21 h. After being stirred for 21 h, precipitate formed during the reaction was separated by atmospheric filtration, and the filtrate was poured into saturated aqueous NH_4Cl solution. The crude product was extracted with Et_2O (20 mL) three times. The combined organic layer was dried over anhydrous sodium sulfate (Na_2SO_4), filtered under atmospheric pressure, and evaporated under reduced pressure using a rotary evaporator. The residue was subjected to silica-gel column chromatography using hexane/EtOAc 20/1 (v/v) mixed solvent as an eluent, followed by recrystallization from CH_2Cl_2/methanol (v/v = 1/1), producing the coupling product **1c** in 63% (0.37 g, 0.63 mmol) as a white solid.

4-Tridecafluorodecyloxy-4'-cyanodiphenylacetylene (1c)

Yield: 63% (white solid); M.p.: T_m = 72 °C, T_c = 158 °C (cooling process); ^{1}H NMR ($CDCl_3$): 1.79–1.97 (m, 4H), 2.10–2.26 (m, 2H), 4.03 (t, J = 6.0 Hz, 2H), 6.88 (d, J = 8.8 Hz, 2H), 7.48 (d, J = 8.8 Hz, 2H), 7.57 (d, J = 8.4 Hz, 2H), 7.63 (d, J = 8.4 Hz, 2H); ^{13}C NMR ($CDCl_3$): δ 17.3, 28.6, 30.6 (t, J = 22.0 Hz), 67.3, 86.8, 94.0, 111.0, 114.4, 114.6, 118.6, 128.6, 131.8, 132.0, 133.4, 159.5 (Carbon signals for C_6F_{13} moiety could not be properly identified because they were complicatedly divided by the coupling with the fluorine nucleus.); ^{19}F NMR ($CDCl_3$, C_6F_6): δ –82.06 (t, J = 10.9 Hz, 3F), –115.5 to –115.9 (m, 2F), –123.1 to –123.4 (m, 2F), –124.1 to –124.3 (m, 2F), –124.7 to –124.9 (m, 2F), –127.3 to –127.5 (m, 2F); IR (KBr): ν 2955, 2883, 2234, 1600, 1512, 1471, 1368, 1284, 1032, 958 cm^{-1}; HRMS (FAB) Calcd for (M^+) $C_{25}H_{16}F_{13}NO$: 593.1024, Found: 593.1029.

NMR spectra

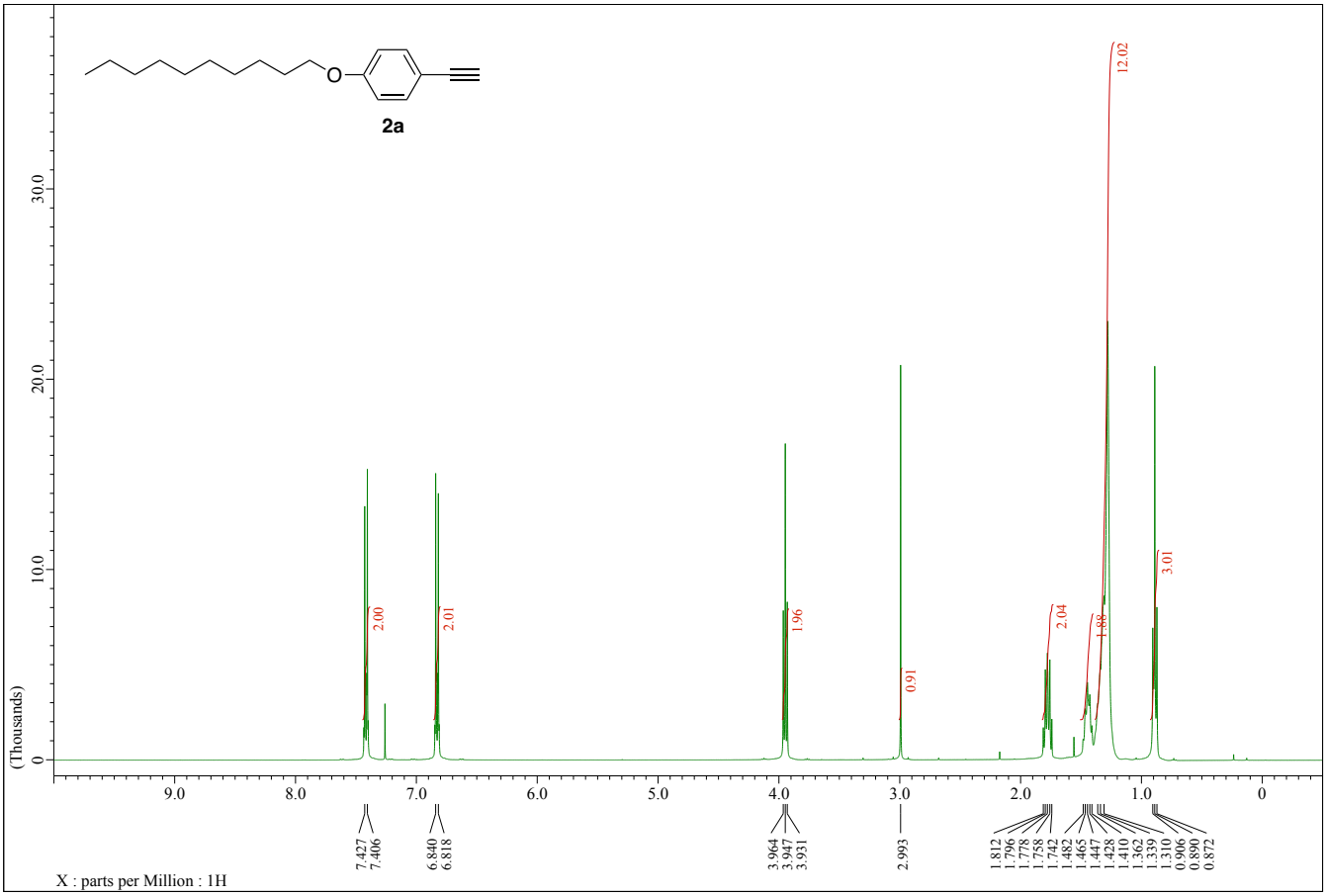

Figure S1. ^{1}H NMR spectrum of **2a** ($CDCl_3$, 400 MHz)

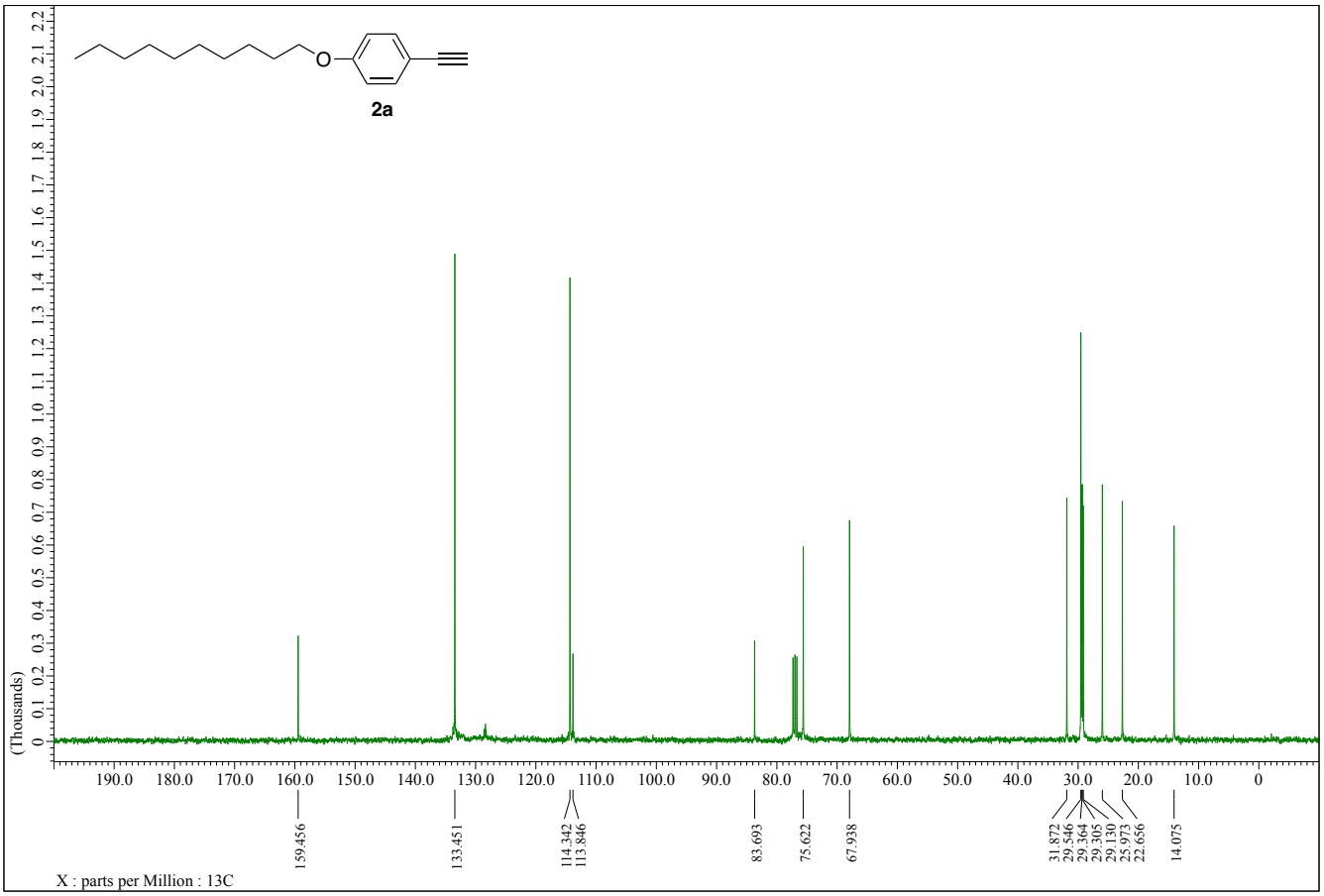

Figure S2. ^{13}C NMR spectrum of **2a** (CDCl3, 100 MHz)

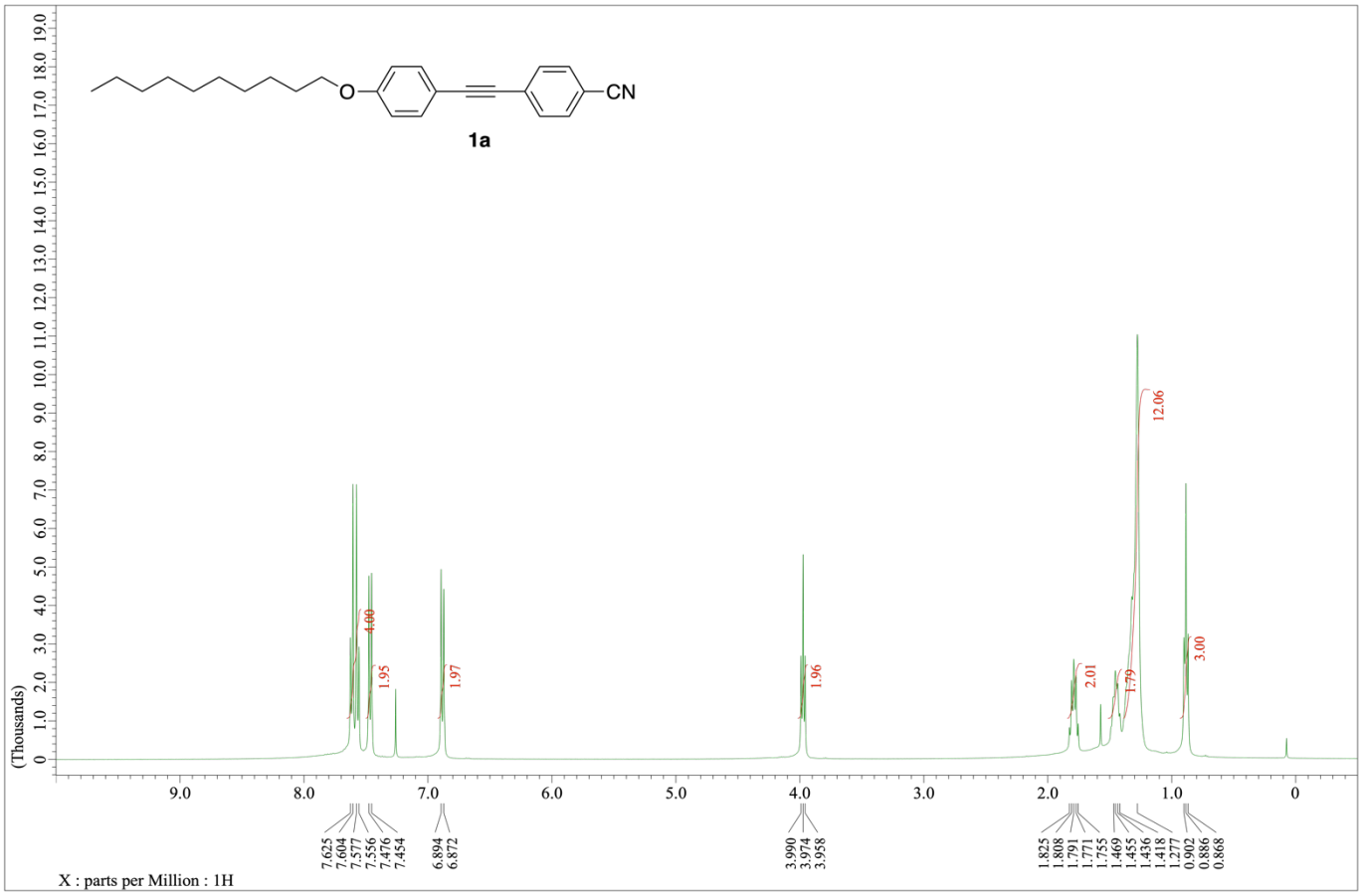

Figure S3. ^{1}H NMR spectrum of **1a** ($CDCl_3$, 400 MHz)

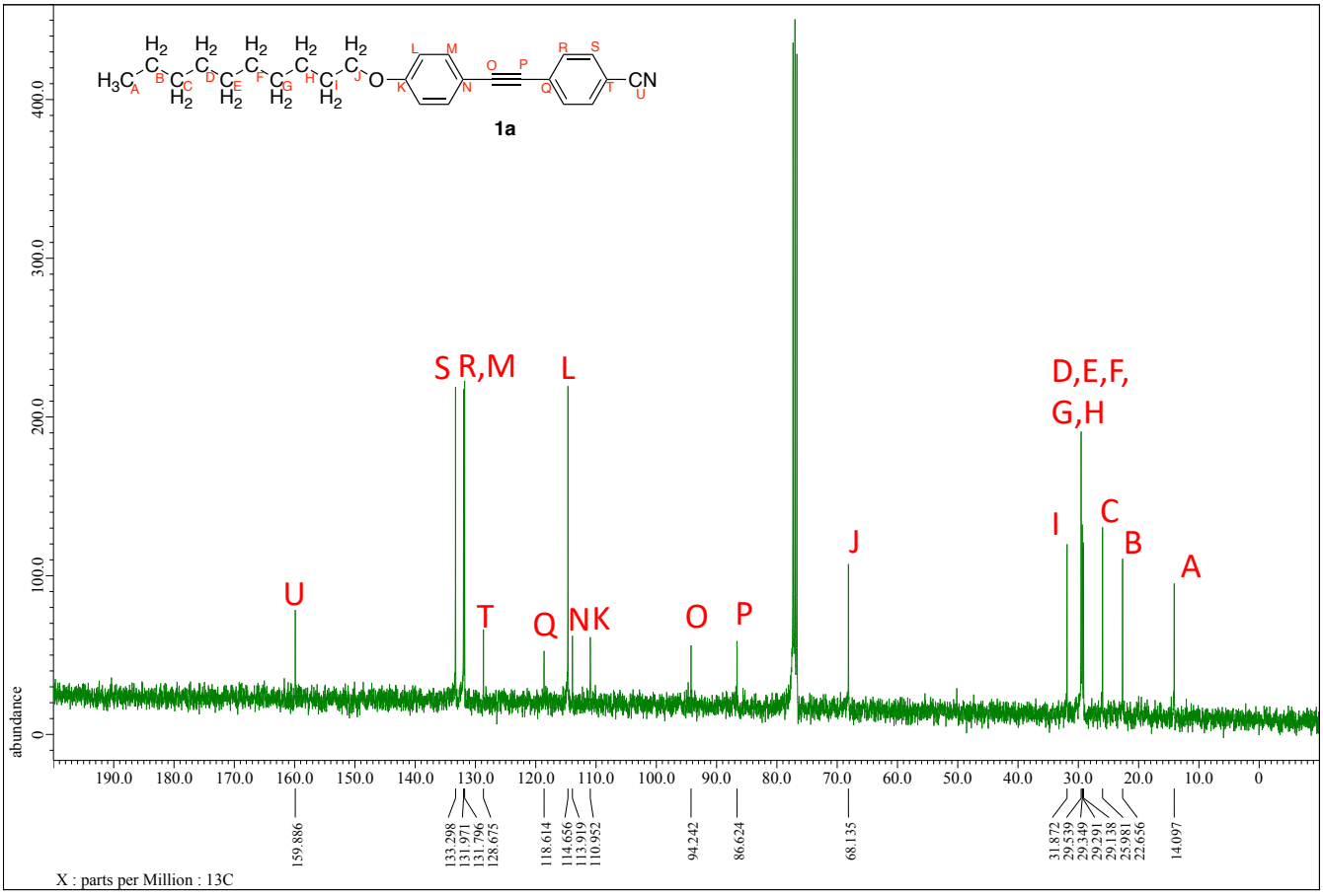

Figure S4. ^{13}C NMR spectrum of **1a** ($CDCl_3$, 100 MHz)

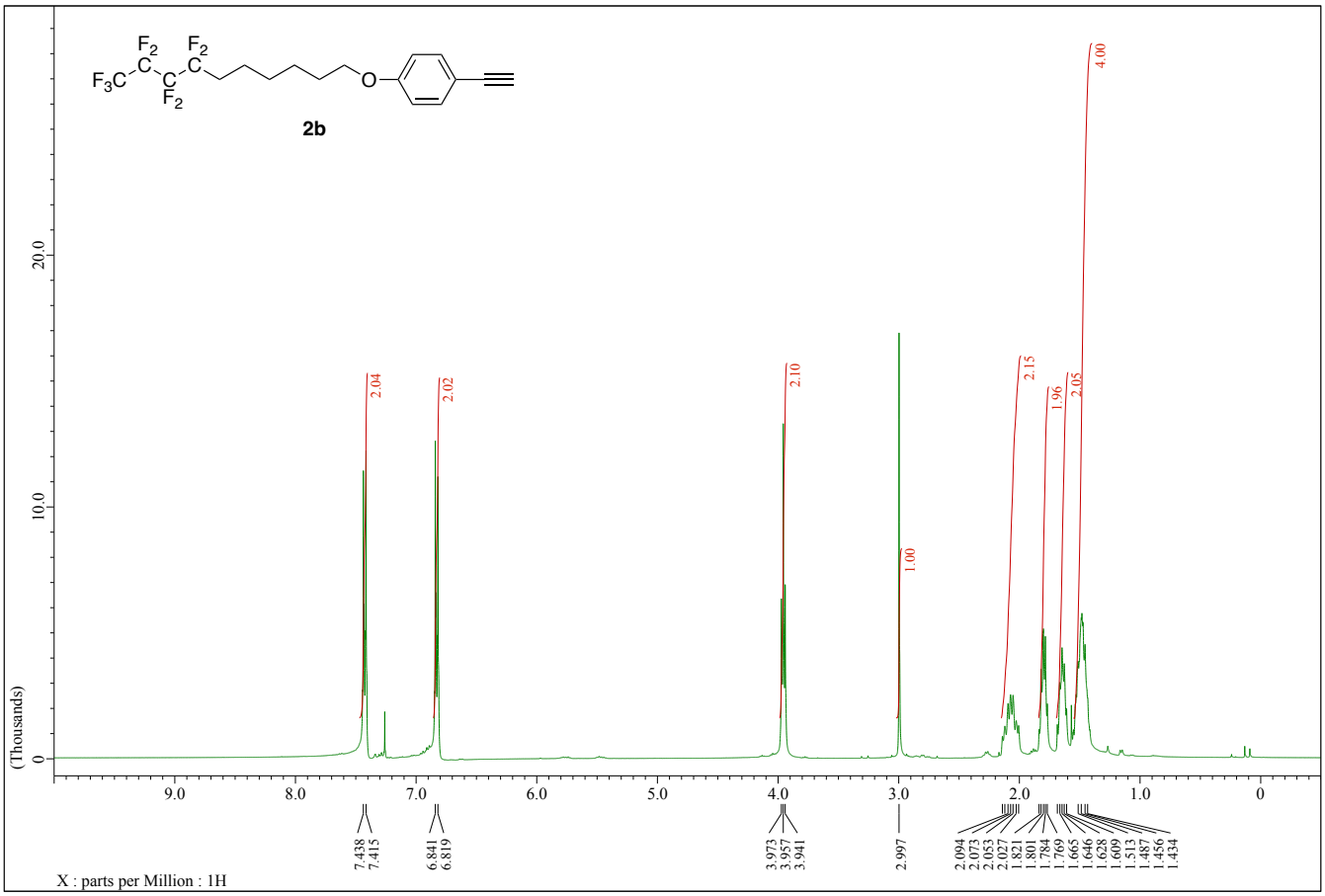

Figure S5. ^{1}H NMR spectrum of **2b** ($CDCl_3$, 400 MHz)

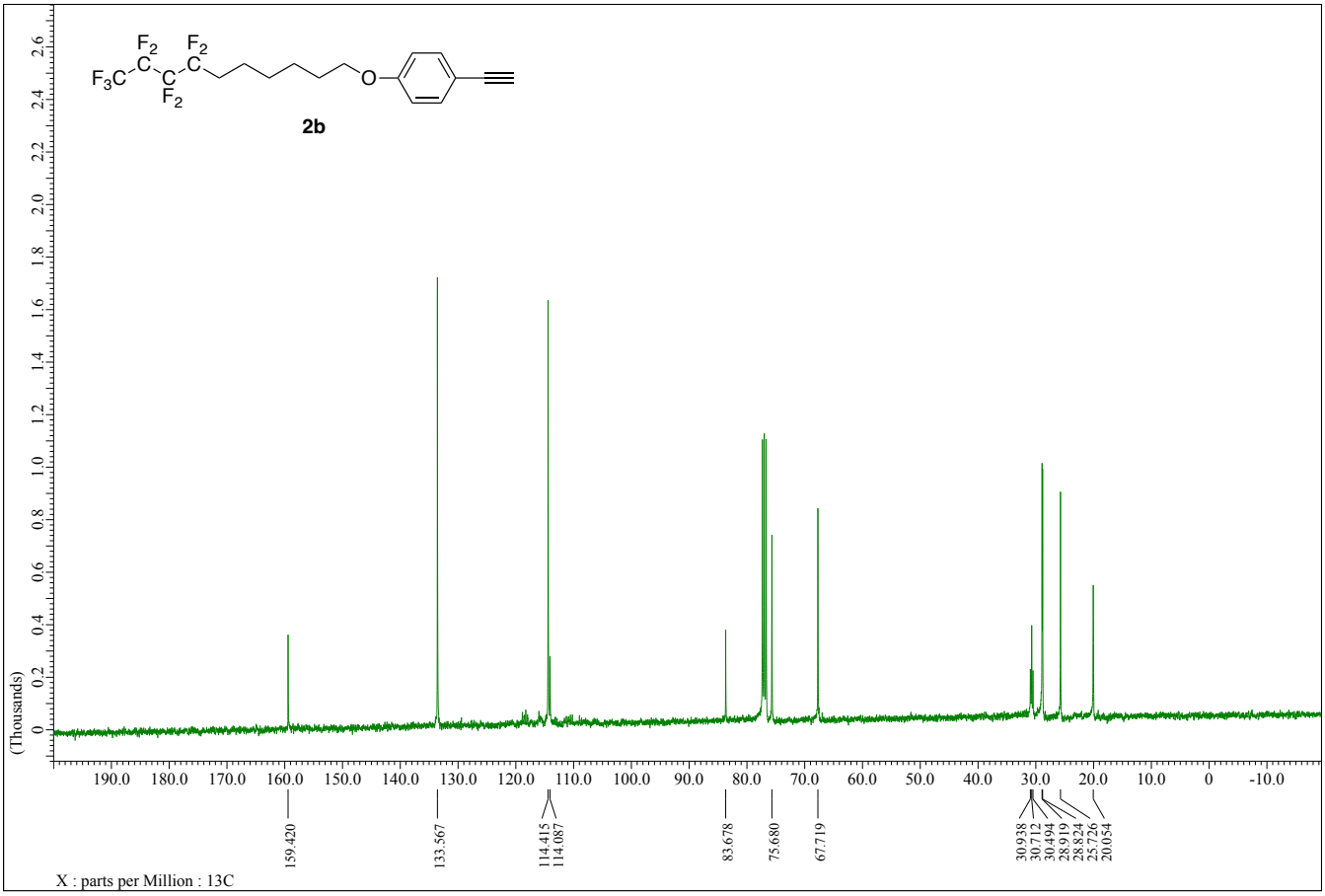

Figure S6. ^{13}C NMR spectrum of **2b** ($CDCl_3$, 100 MHz)

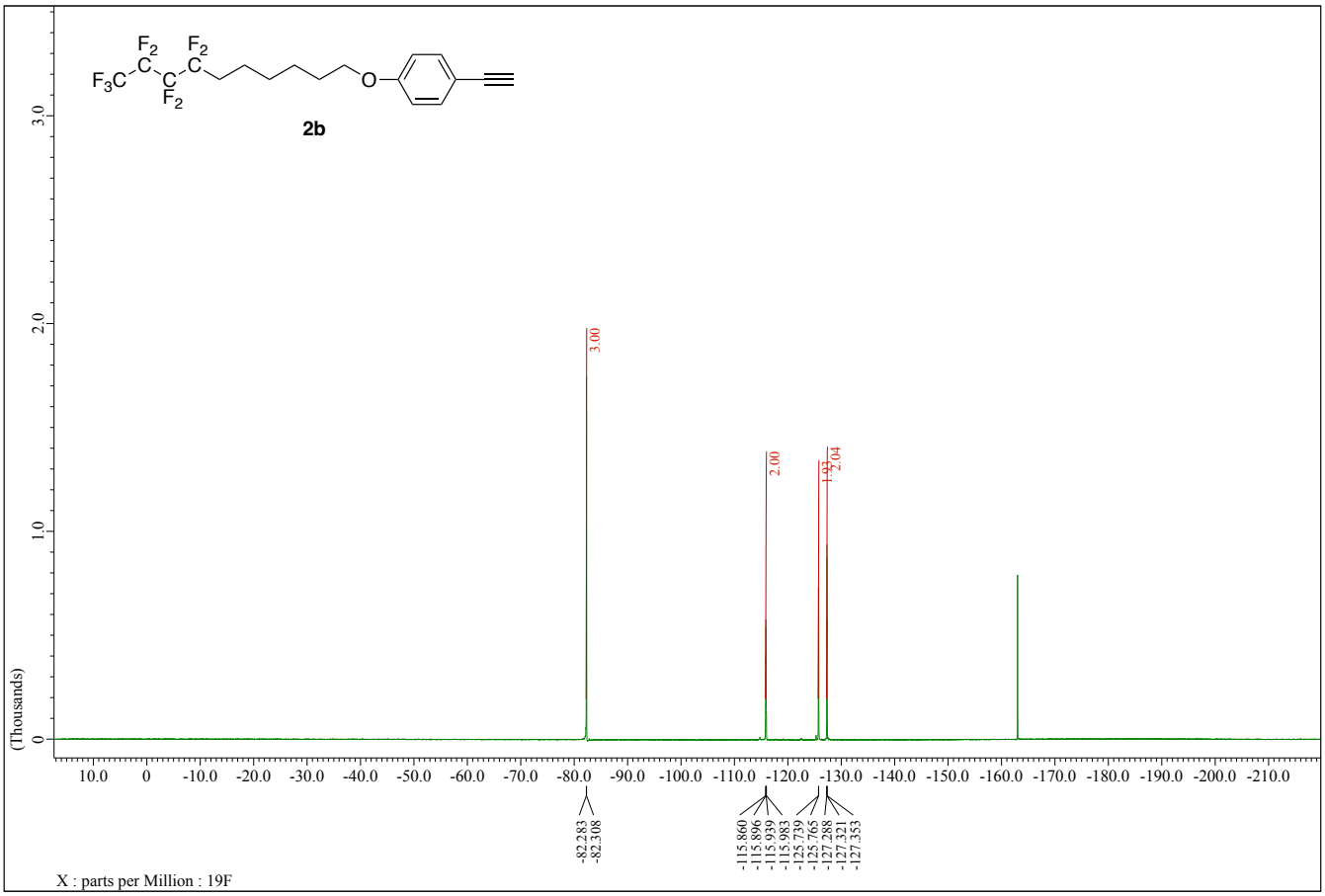

Figure S7. ^{19}F NMR spectrum of **2b** ($CDCl_3$, C_6F_6, 376 MHz)

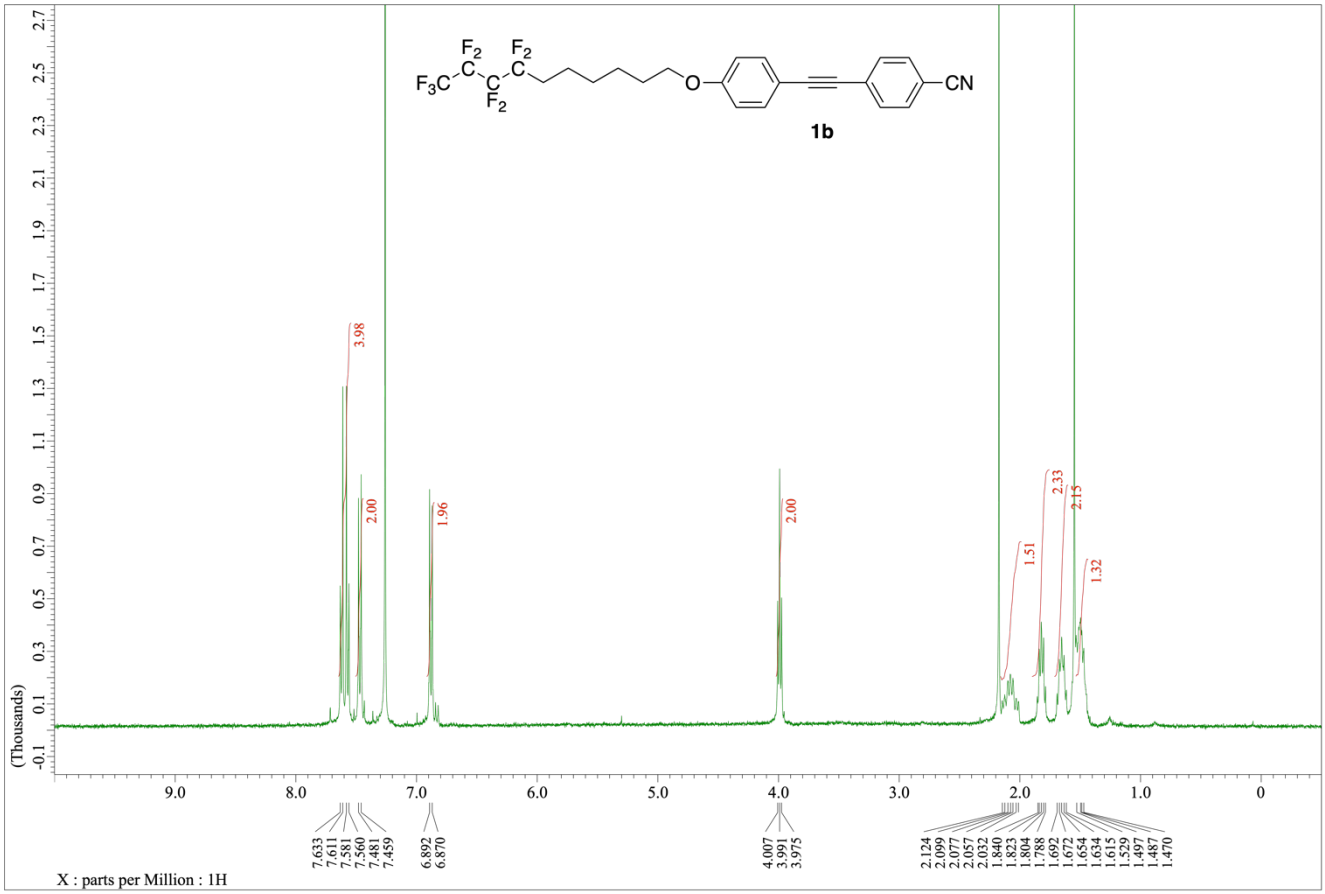

Figure S8. ^{1}H NMR spectrum of **1b** ($CDCl_3$, 400 MHz)

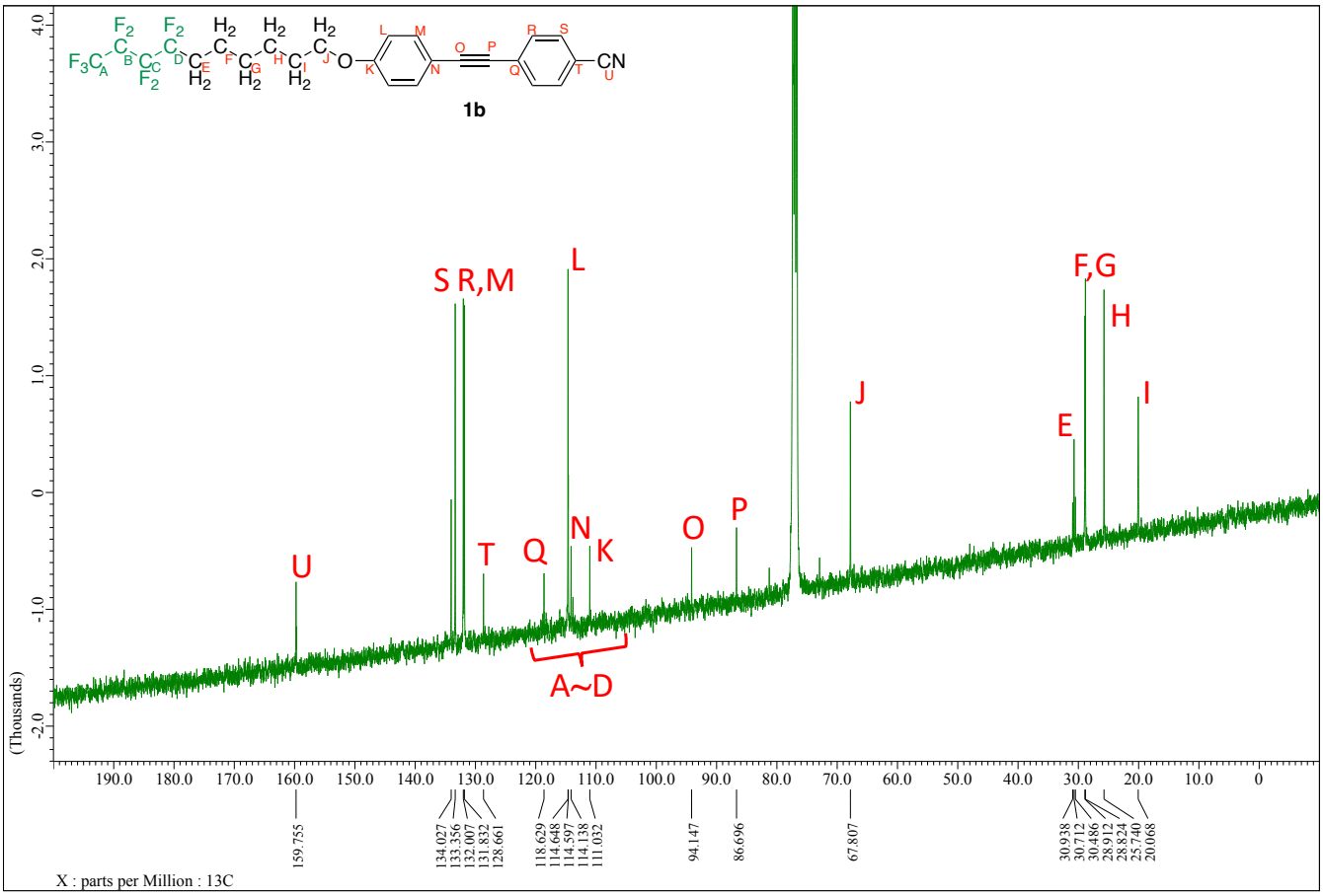

Figure S9. ^{13}C NMR spectrum of **1b** ($CDCl_3$, 100 MHz)

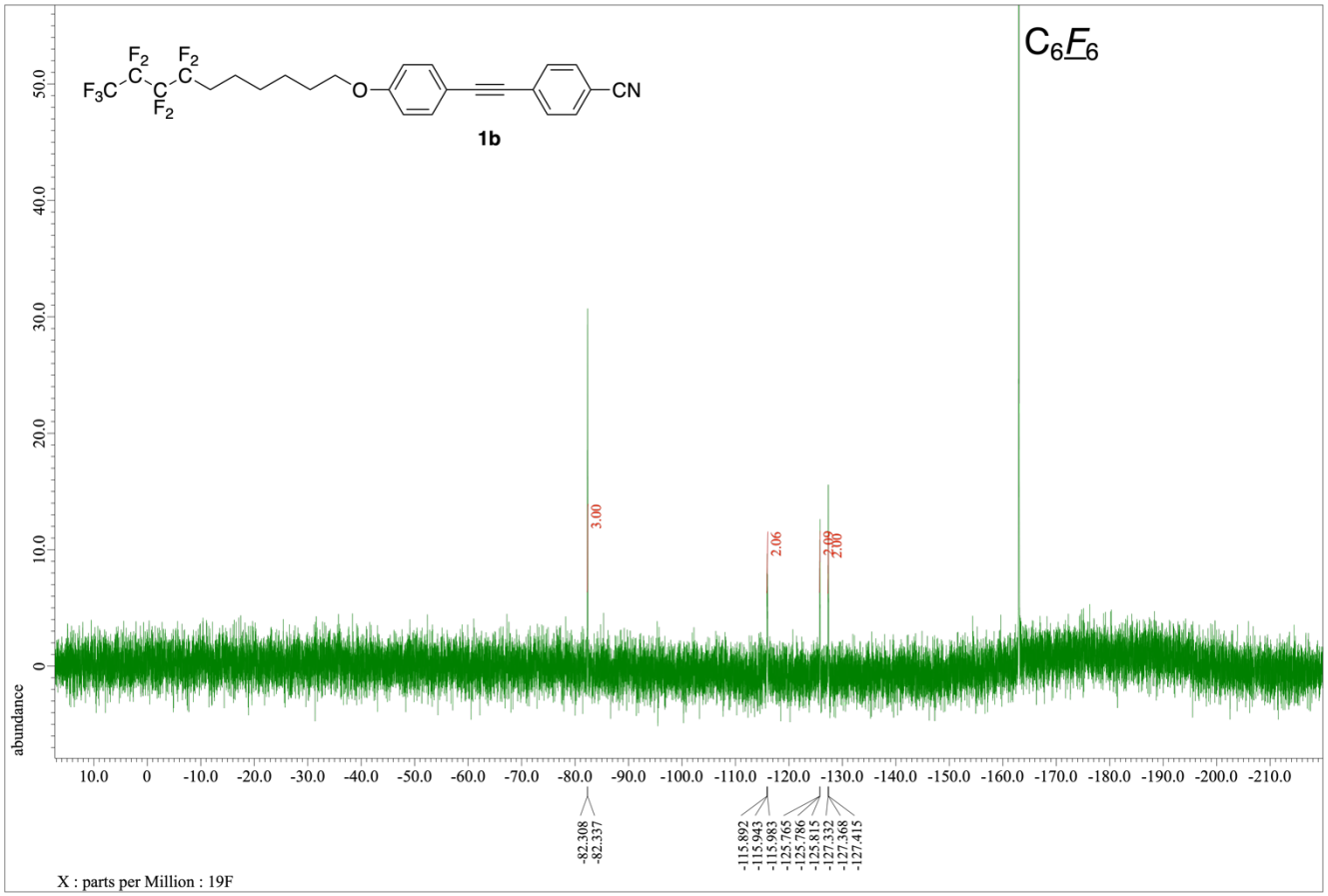

Figure S10. ^{19}F NMR spectrum of **1b** ($CDCl_3$, C_6F_6, 376 MHz)

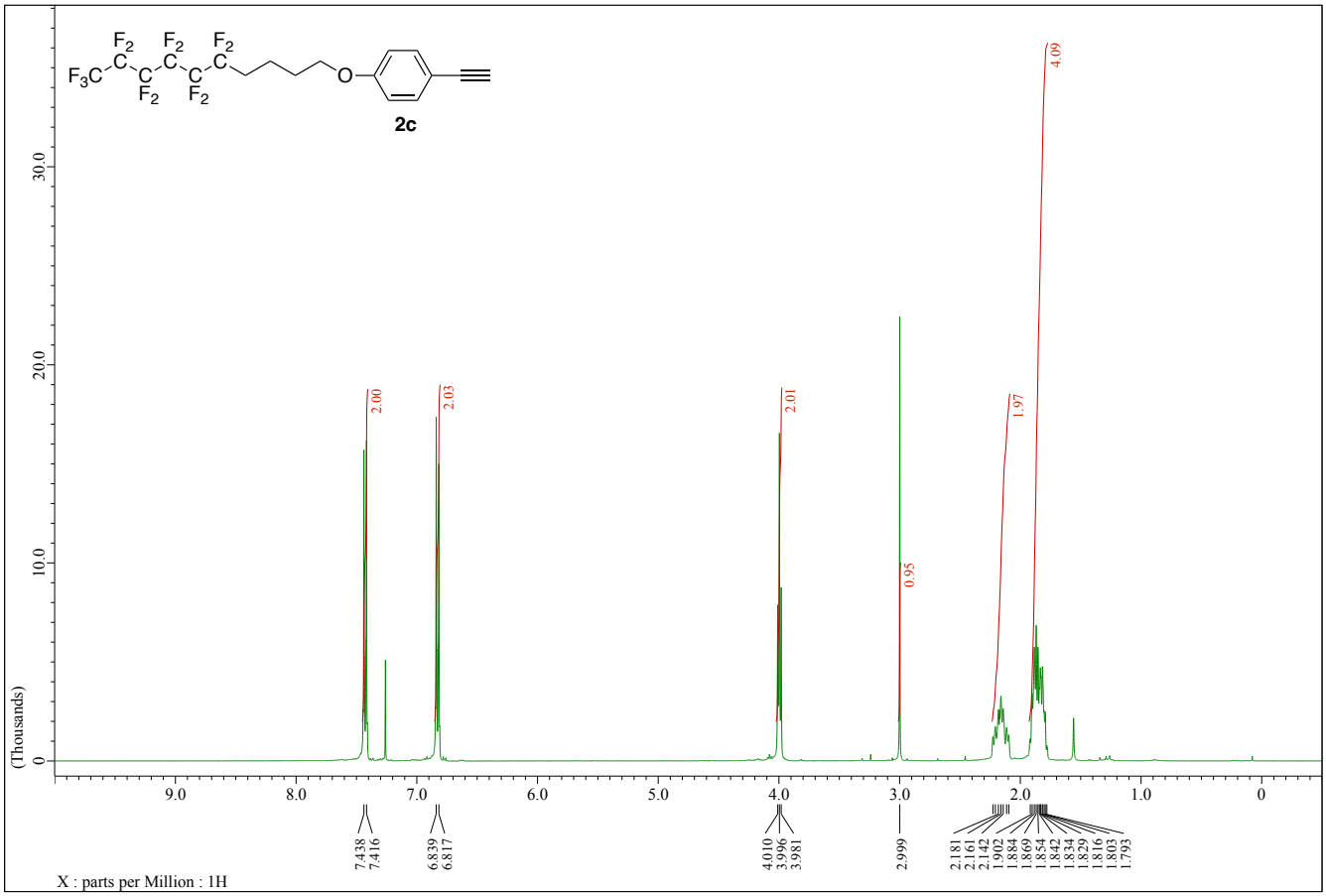

Figure S11. ^{1}H NMR spectrum of **2b** ($CDCl_3$, 400 MHz)

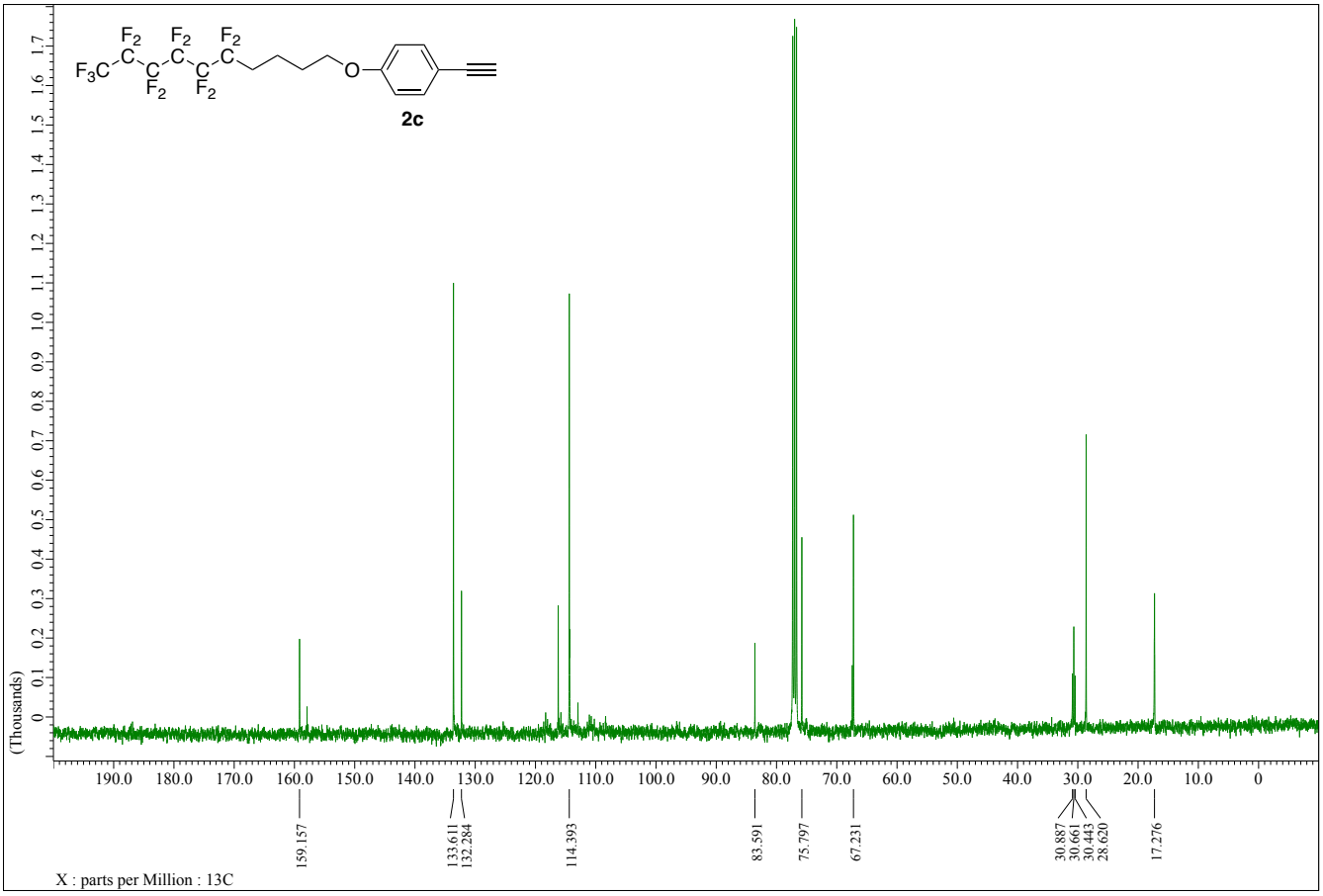

Figure S12. ^{13}C NMR spectrum of **2b** ($CDCl_3$, 100 MHz)

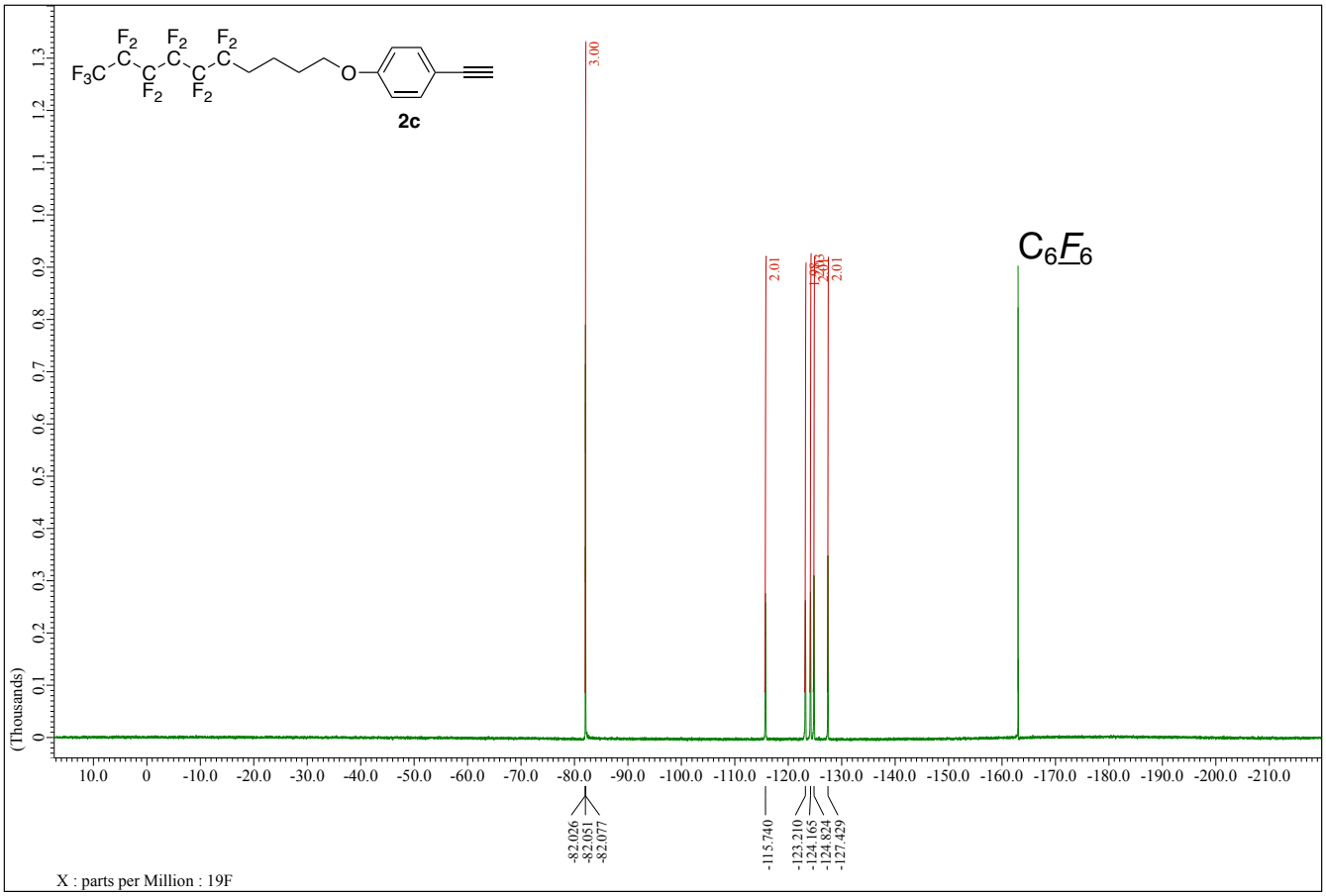

Figure S13. ^{19}F NMR spectrum of **2b** ($CDCl_3$, C_6F_6, 376 MHz)

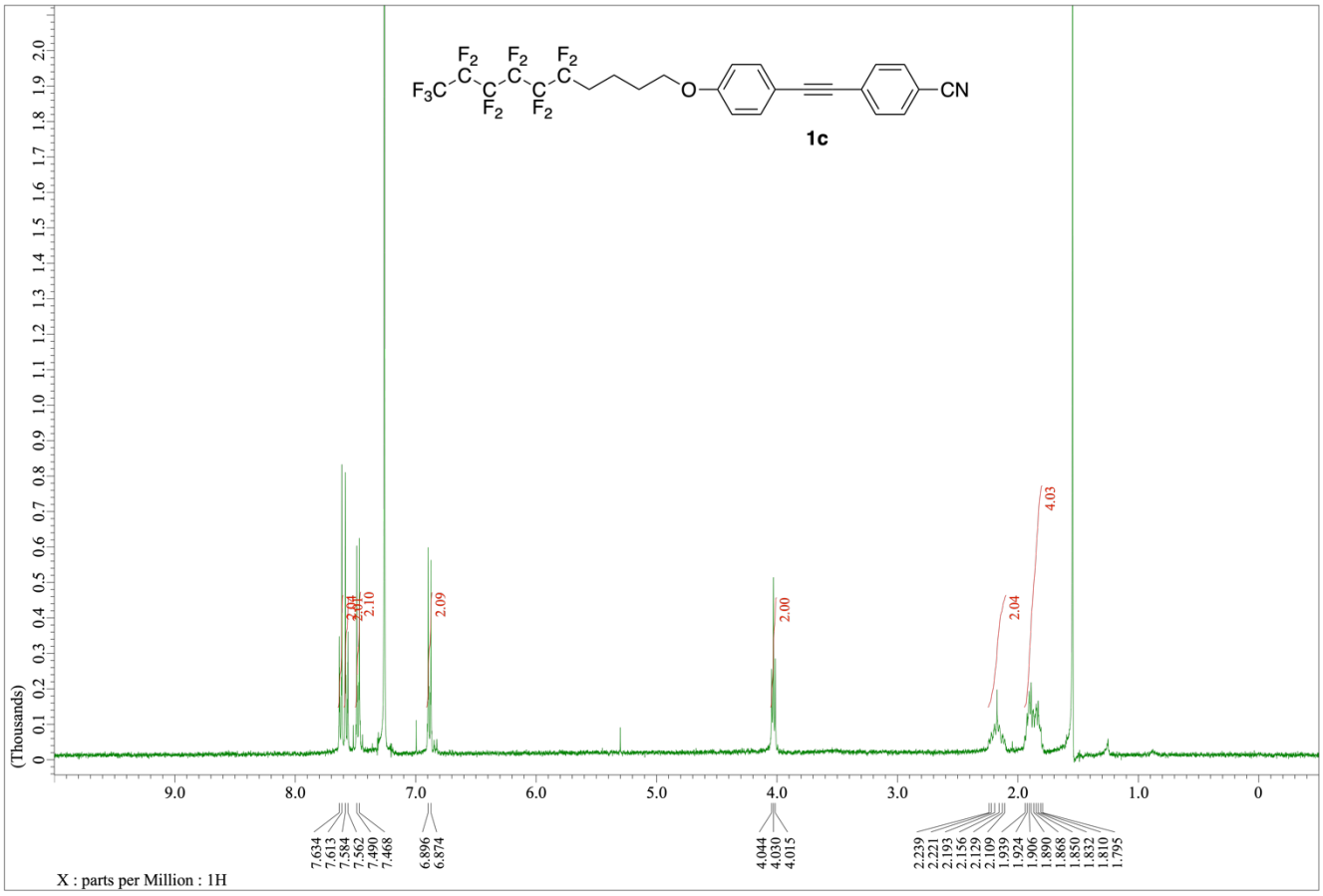

Figure S14. ^{1}H NMR spectrum of **1c** ($CDCl_3$, 400 MHz)

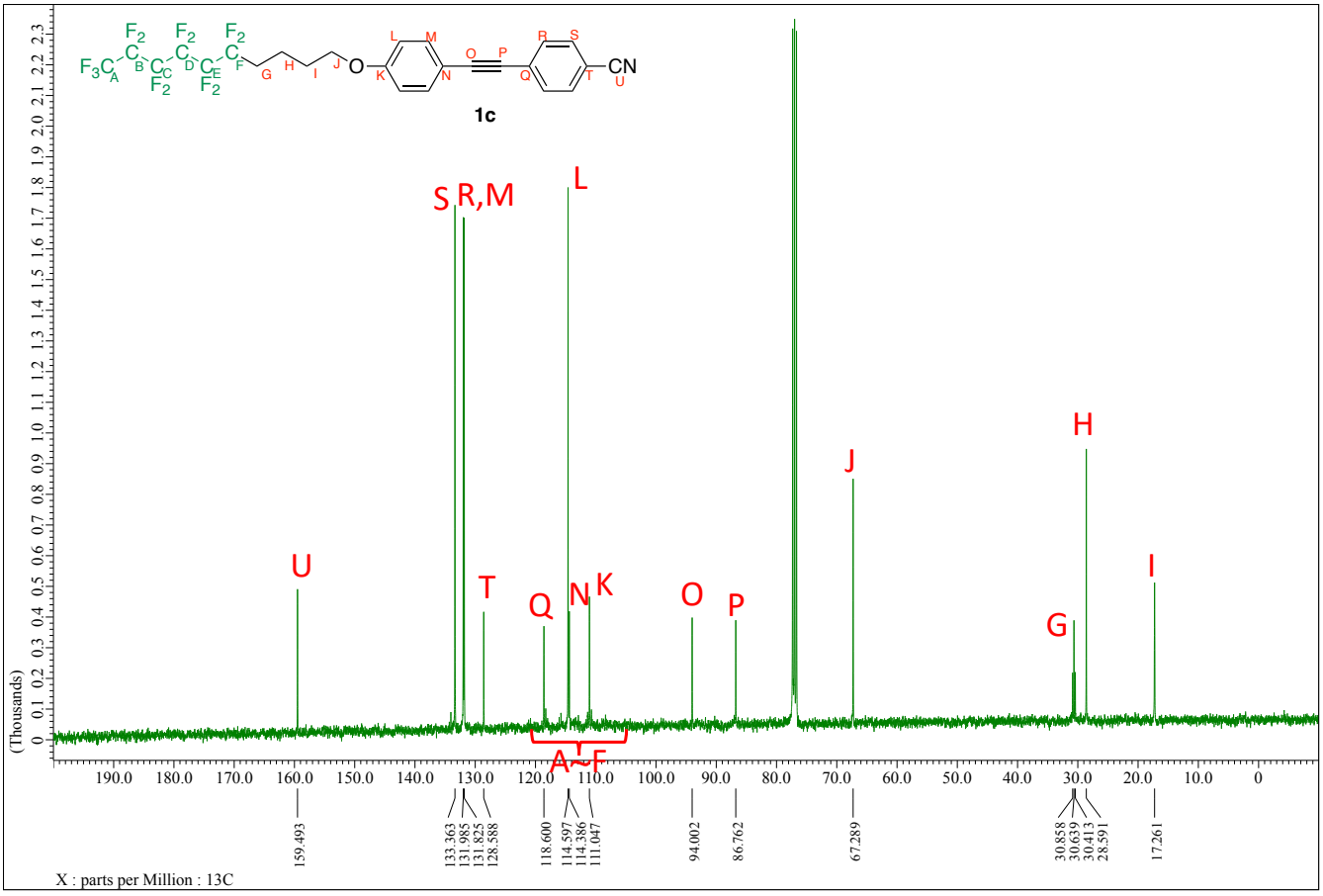

Figure S15. ^{13}C NMR spectrum of **1c** ($CDCl_3$, 100 MHz)

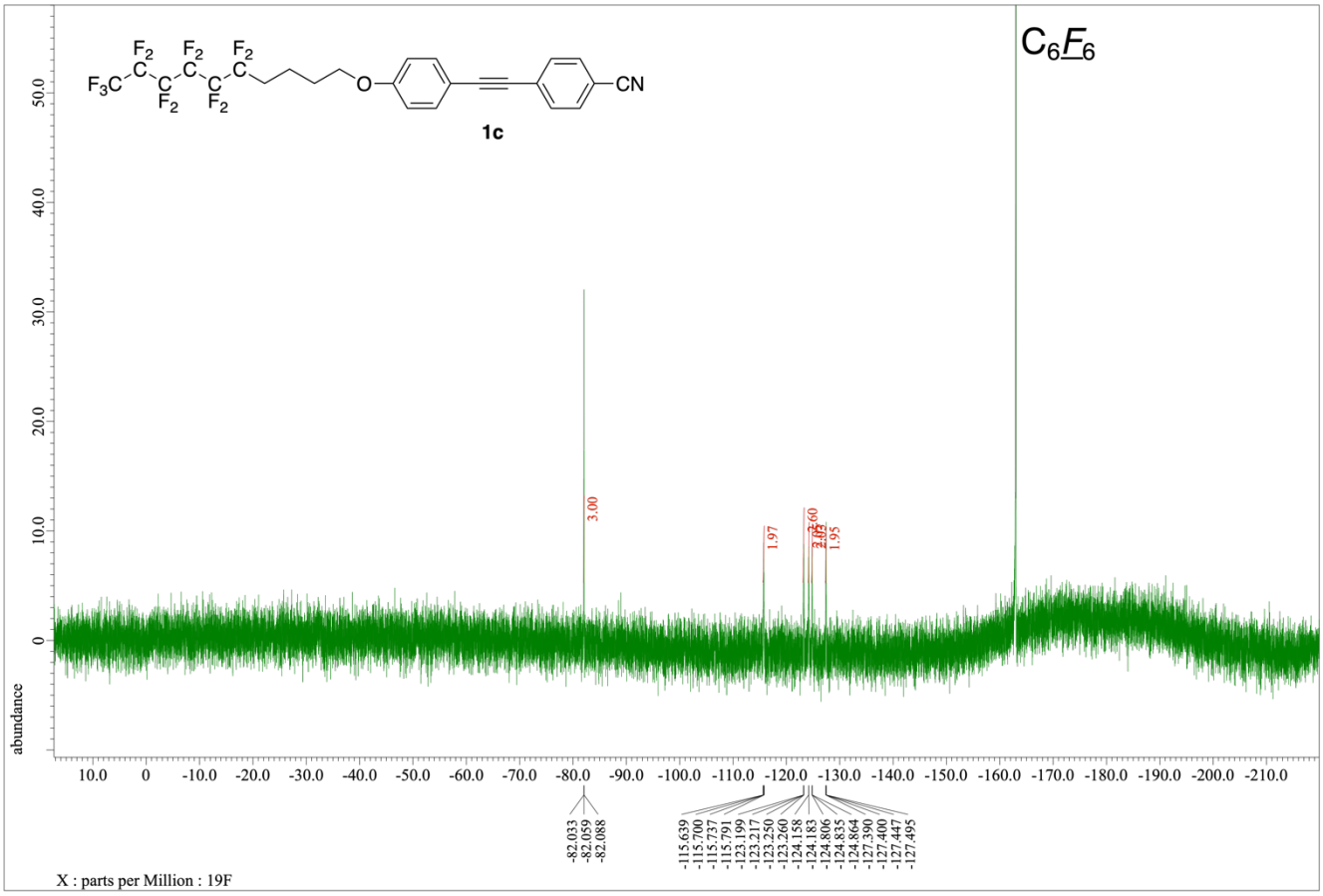

Figure S16. ^{19}F NMR spectrum of **1c** ($CDCl_3$, C_6F_6, 376 MHz)

Theoretical Calculation

Density functional theory (DFT) calculations were carried out using the Gaussian 16 (Rev. B.01) suite of programs. Geometry optimizations were performed at the CAM-B3LYP/6-311+G(d,p)//CAM-B3LYP/6-31+G(d) level of theory with an implicit solvation model, namely, the conductor-like polarizable continuum model (CPCM) for CH2Cl2. Vertical electronic transitions were calculated using a time-dependent DFT (TD-DFT) method at the same level of theory.

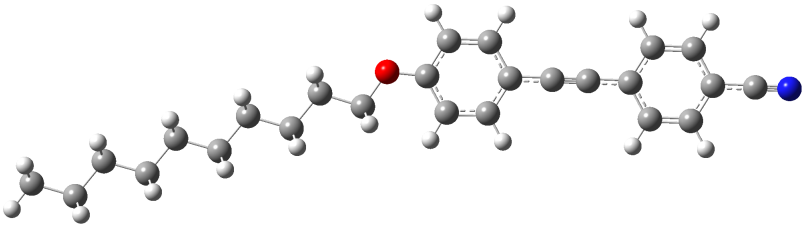

SCF Done: E(RCAM-B3LYP) = -1099.72269713 Hartree

Dipole moment (field-independent basis, Debye):

X= -8.7529 Y= -0.3067 Z= 0.0001 Tot= 8.7583

Figure S17. Optimized geometry of **1a**.

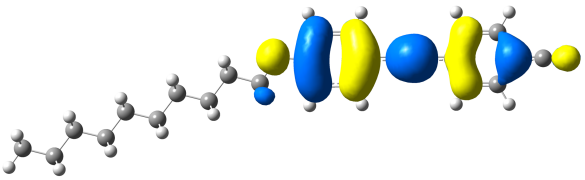

HOMO (–7.35 eV)

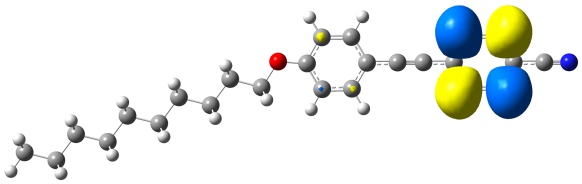

LUMO+1 (0.19 eV)

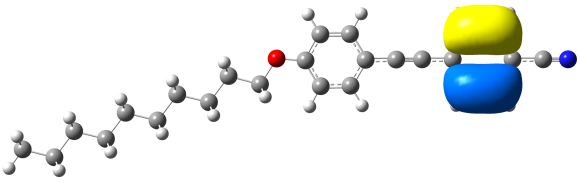

HOMO–3 (–9.26 eV)

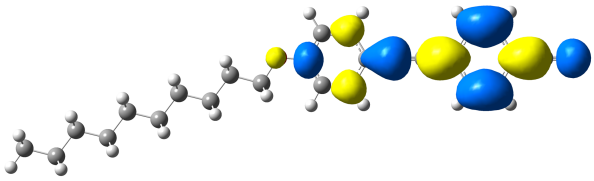

LUMO (–1.17 eV)

Excited State 1: Singlet-A 3.9407 eV 314.62 nm f=1.5355 <S**2>=0.000

97(HOMO) → 98(LUMO) 0.67082 (90%)

Excited State 6: Singlet-A 5.7529 eV 215.52 nm f=0.2368 <S**2>=0.000

94(HOMO–3) → 98(LUMO) 0.44816 (40%)

97(HOMO) → 99(LUMO+1) 0.51824 (54%)

Figure S18. Orbital distributions and the theoretical vertical transition of **1a**.

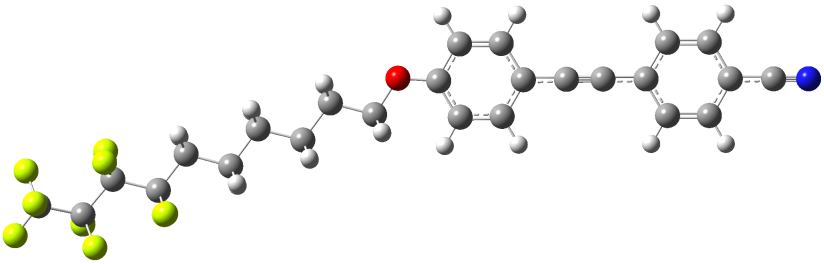

SCF Done: E(RCAM-B3LYP) = -1993.00841978 Hartree

Dipole moment (field-independent basis, Debye):

X= -5.6113 Y= 1.8106 Z= 0.0022 Tot= 5.8962

Figure S19. Optimized geometry of **1b**.

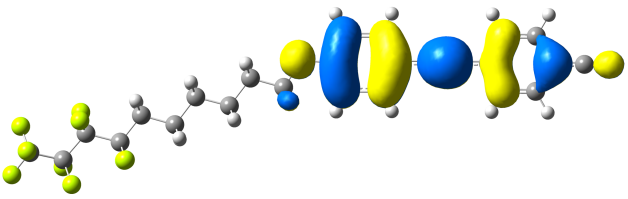

HOMO (–7.36 eV)

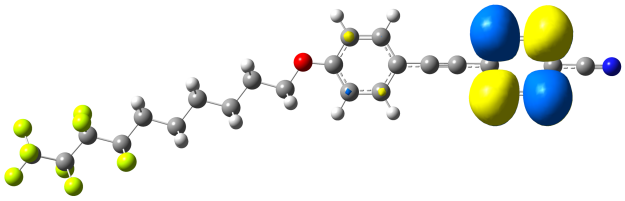

LUMO+1 (0.18 eV)

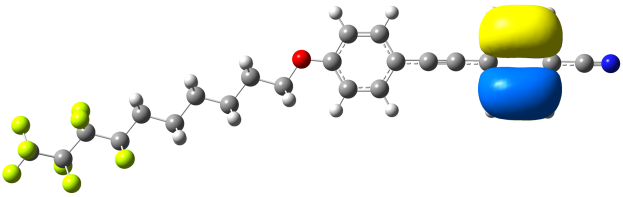

HOMO–3 (–9.26 eV)

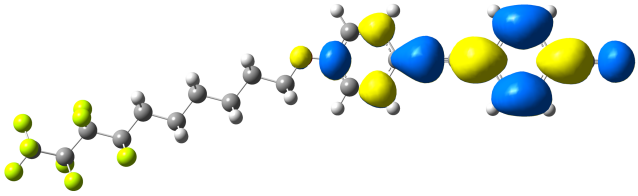

LUMO (–1.18 eV)

Excited State	1:	Singlet-A	3.9446 eV	314.32 nm	f=1.5363	<S**2>=0.000
	133(HOMO) →134(LUMO)		0.67098 (90%)			
Excited State	6:	Singlet-A	5.7564 eV	215.39 nm	f=0.2379	<S**2>=0.000
	130(HOMO–3) →134(LUMO)		0.44706 (40%)			
	133(HOMO) →135(LUMO+1)		0.51878 (54%)			

Figure S20. Orbital distributions and the theoretical vertical transition of **1b**.

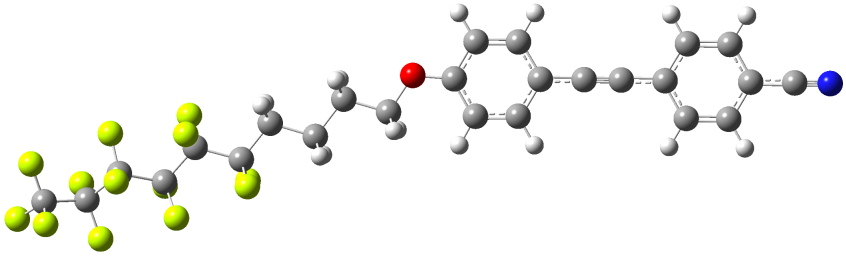

SCF Done: E(RCAM-B3LYP) = -2390.00607031 Hartree

Dipole moment (field-independent basis, Debye):

X= 5.4996 Y= 1.7106 Z= -0.0410 Tot= 5.7596

Figure S21. Optimized geometry of **1c**.

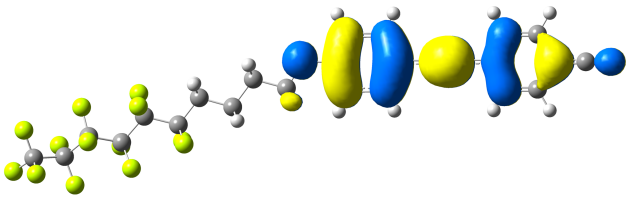

HOMO (–7.38 eV)

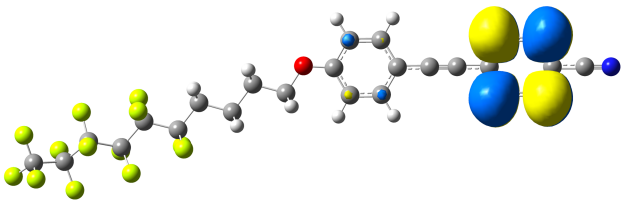

LUMO+1 (0.18 eV)

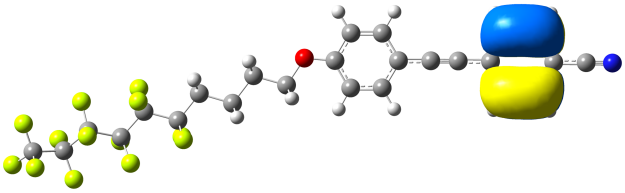

HOMO–3 (–9.27 eV)

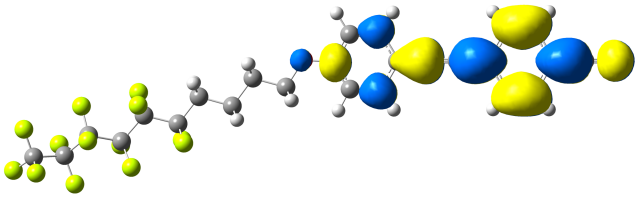

LUMO (–1.19 eV)

Excited State 1: Singlet-A 3.9515 eV 313.77 nm f=1.5367 <S**2>=0.000

149(HOMO) →150(LUMO) 0.67131 (90%)

Excited State 6: Singlet-A 5.7626 eV 215.16 nm f=0.2400 <S**2>=0.000

146(HOMO–3) →150(LUMO) 0.44527 (40%)

149(HOMO) →151(LUMO+1) 0.51971 (54%)

Figure S22. Orbital distributions and the theoretical vertical transition of **1c**.

Cartesian coordinates

Table S1. Cartesian coordinate for optimized geometry of **1a**

No.	Atom No.	Type	Coordinates (Angstroms) x	y	z
1	6	0	1.304159	2.098623	-0.000113
2	6	0	2.665405	1.861389	-0.000138
3	6	0	3.16475	0.546494	-0.00005
4	6	0	2.251689	-0.513712	0.000056
5	6	0	0.880196	-0.283743	0.000085
6	6	0	0.400153	1.028299	0.000011
7	1	0	0.914633	3.11148	-0.000185
8	1	0	3.358288	2.696673	-0.000229
9	1	0	2.619329	-1.534865	0.000118
10	1	0	0.202747	-1.128302	0.000157
11	6	0	4.571419	0.298285	-0.000067
12	6	0	5.763731	0.085156	-0.000072
13	6	0	7.168044	-0.172636	-0.000063
14	6	0	7.64603	-1.492898	-0.000122
15	6	0	8.086763	0.889134	0.000012
16	6	0	9.007361	-1.747382	-0.000097
17	1	0	6.941034	-2.316904	-0.000181
18	6	0	9.449136	0.639363	0.000034
19	1	0	7.72349	1.910924	0.000052
20	6	0	9.913941	-0.680949	-0.000015
21	1	0	9.371665	-2.768865	-0.000135
22	1	0	10.15507	1.462755	0.000089
23	8	0	-0.913104	1.361639	0.000024
24	6	0	-1.894086	0.321842	0.000201
25	1	0	-1.758727	-0.305098	-0.889812
26	1	0	-1.758732	-0.304789	0.890441
27	6	0	-3.264141	0.969737	0.000062
28	1	0	-3.351362	1.615778	-0.882026
29	1	0	-3.35139	1.616105	0.881907
30	6	0	-4.387403	-0.066728	0.00023
31	1	0	-4.285526	-0.717045	0.8799
32	1	0	-4.285477	-0.717374	-0.879191
33	6	0	-5.779454	0.563587	0.000069
34	1	0	-5.882065	1.214557	-0.879349
35	1	0	-5.882151	1.214827	0.879276
36	6	0	-6.907708	-0.466723	0.000166
37	1	0	-6.803152	-1.118058	0.879442
38	1	0	-6.803064	-1.118312	-0.878911
39	6	0	-8.30189	0.158652	0.000003
40	1	0	-8.406579	0.810093	-0.879221
41	1	0	-8.406689	0.810316	0.879049
42	6	0	-9.430053	-0.872052	0.00006
43	1	0	-9.324999	-1.523575	0.879259
44	1	0	-9.324888	-1.523788	-0.878968
45	6	0	-10.824987	-0.248571	-0.000106
46	1	0	-10.931332	0.402912	-0.879316
47	1	0	-10.931455	0.403109	0.878944
48	6	0	-11.953335	-1.279168	-0.000071
49	1	0	-11.847599	-1.929834	0.878439
50	1	0	-11.847476	-1.930026	-0.878423
51	6	0	-13.342938	-0.645429	-0.000238
52	1	0	-13.488018	-0.014443	-0.885012
53	1	0	-14.131095	-1.406032	-0.00021
54	1	0	-13.488143	-0.014251	0.884379
55	6	0	11.324402	-0.942622	0.000021
56	7	0	12.463055	-1.154109	0.000052

Table S2. Cartesian coordinate for optimized geometry of **1b**

No.	Atom No.	Type	Coordinates (Angstroms) x	y	z
1	6	0	4.543771	2.195921	-0.047522
2	6	0	5.898864	1.925599	-0.038491
3	6	0	6.365957	0.599234	-0.01039
4	6	0	5.427362	-0.438217	0.008596
5	6	0	4.061892	-0.174895	-0.00006
6	6	0	3.614175	1.148078	-0.028596
7	1	0	4.179142	3.217781	-0.069296
8	1	0	6.611937	2.74358	-0.053306
9	1	0	5.769844	-1.467853	0.030501
10	1	0	3.364165	-1.002632	0.015328
11	6	0	7.766121	0.316754	-0.001653
12	6	0	8.952743	0.074191	0.005439
13	6	0	10.350137	-0.218697	0.013453
14	6	0	10.79467	-1.550527	0.025774
15	6	0	11.29528	0.819574	0.008909
16	6	0	12.149152	-1.839287	0.033217
17	1	0	10.069118	-2.356497	0.029297
18	6	0	12.65091	0.535503	0.016375
19	1	0	10.95805	1.850225	-0.000501
20	6	0	13.082301	-0.796035	0.028509
21	1	0	12.487472	-2.86964	0.042597
22	1	0	13.377376	1.340825	0.012853
23	8	0	2.309021	1.513123	-0.040039
24	6	0	1.303987	0.497618	-0.018539
25	1	0	1.425867	-0.1535	-0.892955
26	1	0	1.421295	-0.110737	0.886827
27	6	0	-0.049627	1.179243	-0.038832
28	1	0	-0.12085	1.800704	-0.939682
29	1	0	-0.121162	1.852839	0.823672
30	6	0	-1.196571	0.169744	-0.008811
31	1	0	-1.116036	-0.450054	0.894347
32	1	0	-1.106914	-0.513699	-0.863947
33	6	0	-2.570816	0.836538	-0.040656
34	1	0	-2.656526	1.450122	-0.947404
35	1	0	-2.661775	1.524289	0.810731
36	6	0	-3.715071	-0.175702	-0.0006
37	1	0	-3.635433	-0.781659	0.908602
38	1	0	-3.627059	-0.861118	-0.851225
39	6	0	-5.079134	0.516889	-0.039984
40	1	0	-5.175983	1.119973	-0.947178
41	1	0	-5.192304	1.190425	0.815931
42	6	0	-6.227615	-0.462754	-0.010791
43	6	0	-7.625543	0.20761	0.017503
44	6	0	-8.83853	-0.735468	-0.218936
45	6	0	-10.214352	-0.138903	0.186901
46	6	0	14.485782	-1.092968	0.036081
47	7	0	15.618753	-1.332914	0.042172
48	9	0	-11.181806	-0.942643	-0.260537
49	9	0	-10.32165	-0.045649	1.512428
50	9	0	-10.382909	1.07262	-0.349198
51	9	0	-8.680615	-1.878133	0.479464
52	9	0	-8.903434	-1.035994	-1.531232
53	9	0	-7.778238	0.811611	1.220738
54	9	0	-7.669094	1.164215	-0.939179
55	9	0	-6.150555	-1.269602	1.088496
56	9	0	-6.199337	-1.286673	-1.103364

Table S3. Cartesian coordinate for optimized geometry of **1c**

No.	Atom No.	Type	Coordinates (Angstroms) x	y	z
1	6	0	-5.022642	2.169388	0.077476
2	6	0	-6.379371	1.907405	0.061921
3	6	0	-6.854327	0.584105	0.025313
4	6	0	-5.922239	-0.459118	0.005963
5	6	0	-4.555183	-0.204234	0.021635
6	6	0	-4.100135	1.115745	0.056933
7	1	0	-4.651723	3.188811	0.105234
8	1	0	-7.087459	2.729654	0.077635
9	1	0	-6.270957	-1.486477	-0.021981
10	1	0	-3.862606	-1.036327	0.005989
11	6	0	-8.256218	0.310338	0.007201
12	6	0	-9.444206	0.075239	-0.009244
13	6	0	-10.84337	-0.208833	-0.029578
14	6	0	-11.295786	-1.537132	-0.078444
15	6	0	-11.78217	0.834766	-0.001338
16	6	0	-12.651948	-1.817266	-0.098625
17	1	0	-10.575088	-2.347145	-0.100555
18	6	0	-13.139457	0.559324	-0.021382
19	1	0	-11.438725	1.862706	0.036441
20	6	0	-13.57877	-0.768779	-0.070115
21	1	0	-12.996471	-2.8449	-0.136486
22	1	0	-13.861042	1.368732	0.000568
23	8	0	-2.791993	1.473085	0.073266
24	6	0	-1.795002	0.452112	0.04979
25	1	0	-1.916524	-0.198106	0.924861
26	1	0	-1.915371	-0.155939	-0.855207
27	6	0	-0.439577	1.131533	0.066153
28	1	0	-0.366598	1.758733	0.962254
29	1	0	-0.365234	1.796757	-0.802074
30	6	0	0.698213	0.111302	0.044724
31	1	0	0.610871	-0.521904	-0.844575
32	1	0	0.621193	-0.546684	0.917432
33	6	0	2.061142	0.806548	0.046928
34	1	0	2.162843	1.448665	0.926083
35	1	0	2.16951	1.441046	-0.838751
36	6	0	3.207646	-0.176646	0.056838
37	6	0	4.605714	0.489925	-0.031592
38	6	0	5.817942	-0.442951	0.26378
39	6	0	7.178656	0.115146	-0.254468
40	6	0	8.420634	-0.551236	0.406708
41	6	0	9.753616	-0.329661	-0.36052
42	6	0	-14.983959	-1.05688	-0.090944
43	7	0	-16.118301	-1.289697	-0.107817
44	9	0	10.763737	-0.74409	0.405461
45	9	0	9.768872	-1.02399	-1.497304
46	9	0	9.925627	0.965176	-0.636898
47	9	0	8.222322	-1.881839	0.497869
48	9	0	8.575168	-0.046003	1.644167
49	9	0	7.242237	-0.08178	-1.587022
50	9	0	7.238758	1.43955	-0.009197
51	9	0	5.616074	-1.643138	-0.314094
52	9	0	5.908333	-0.615405	1.599397
53	9	0	4.748415	1.001564	-1.277628
54	9	0	4.653949	1.512198	0.852678
55	9	0	3.110729	-1.045414	-0.991701
56	9	0	3.193802	-0.934081	1.196611

Phase transition behavior

The phase transition behavior was observed by polarized optical microscopy using an Olympus BX53 microscope, equipped with a heating and cooling stage (Linkam Scientific Instruments, 10.0002L). The phase sequences and the phase transition enthalpies (ΔH) and entropies (ΔS) were determined using a differential scanning calorimetry (SHIMADZU DSC-60 Plus) at heating and cooling rates of 5.0 °C min^{-1} under N_2 atmosphere. Powder X-ray diffraction patterns were measured using an X-ray diffractometer (Rigaku MiniFlex600) equipped with an X-ray tube (Cu$K\alpha$, l = 1.54 Å) and semiconductor detector (D/teX Ultra2). The sample powder was mounted on a silicon non-reflecting plate, and the plate was set on a benchtop stage (Anton Paar, BTS-500). Temperature, heating/cooling rate, and time of X-ray exposure were precisely controlled.

(a)

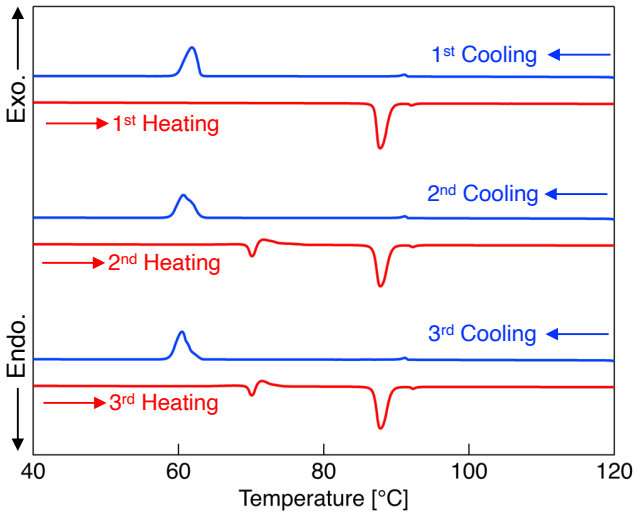

(b)

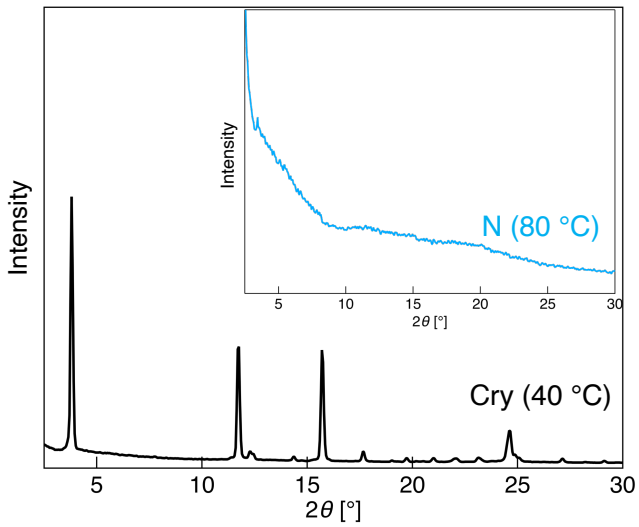

(c)

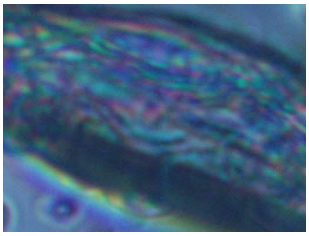

Figure S23. (a) DSC thermograms of **1a** during the heating and cooling processes under N_2 atmosphere. Scan rate: 5.0 °C min^{-1}. (b) Powder X-ray diffraction patterns of **1a** measured at 40 °C in Cry and 80 °C in N phases. (c) Optical texture image of 1a at 91 °C during the cooling process.

Table S4. Phase sequence of **1a** and the phase-transition enthalpy and entropy

1a	Phase sequence	Phase transition temperature [°C]	ΔH [kJ mol^{-1}]	ΔS [J mol^{-1} K^{-1}]
1st Heating	Cr–N	87	44.16	122.72
	N–Iso	92	0.80	2.21
1st Cooling	N–Iso	92	–1.09	–3.00
	Cr–N	63	–38.26	–113.82
2nd Heating	Cr^1–Cr^2	69	–2.44	–7.13
	Cr^2–N	87	43.98	–122.23
	N–Iso	92	0.86	2.36
2nd Cooling	N–Iso	92	–1.17	–3.20
	Cr–N	63	–39.72	–118.19
3rd Heating	Cr^1–Cr^2	69	–1.22	–3.55
	Cr^2–N	87	43.94	122.13
	N–Iso	91	0.80	2.20
3rd Cooling	N–Iso	92	–1.10	–3.01
	Cr–N	62	–38.38	–114.53

(a)

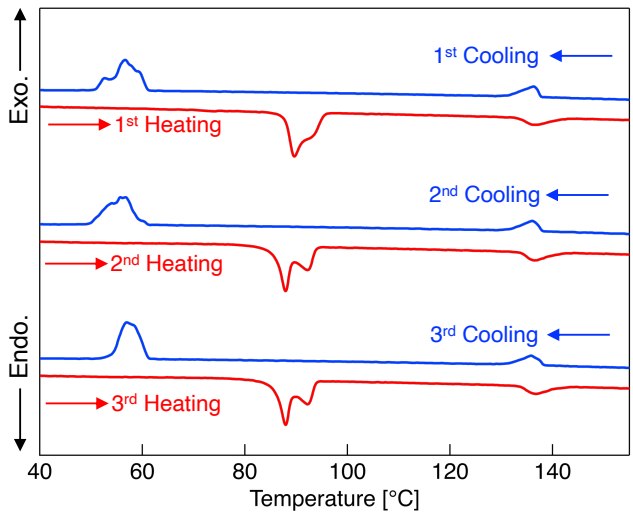

(b)

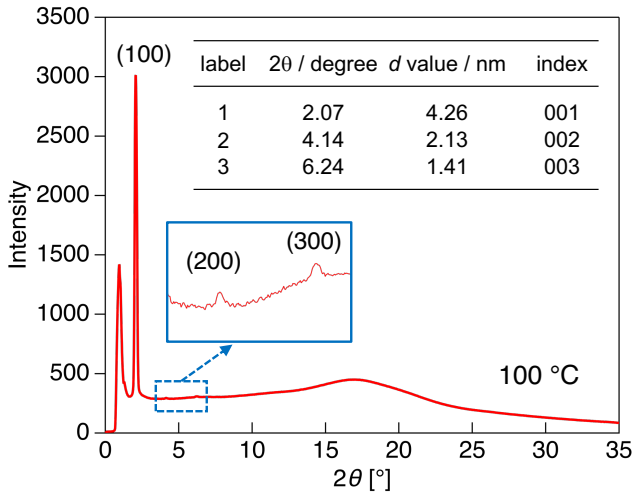

label	2θ / degree	d value / nm	index
1	2.07	4.26	001
2	4.14	2.13	002
3	6.24	1.41	003

(c)

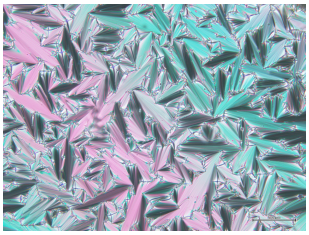

Figure S24. (a) DSC thermograms of **1b** during the heating and cooling processes under N_2 atmosphere. Scan rate: 5.0 °C min^{-1}. (b) Powder X-ray diffraction patterns of **1b** measured at 100 °C in SmA phases. (c) Optical texture image of **1b** at 100 °C during the cooling process.

Table S5. Phase sequence of **1b** and the phase-transition enthalpy and entropy

1b	Phase sequence	Phase transition temperature [°C]	ΔH [kJ mol^{-1}]	ΔS [J mol^{-1} K^{-1}]
1st Heating	Cr–SmA	88	27.76	76.92
	SmA–Iso	133	5.37	13.23
1st Cooling	SmA–Iso	138	–5.59	–13.62
	Cr–SmA	61	–23.07	–69.07
2nd Heating	Cr^1–Cr^2	85		
	Cr^2–SmA	92	27.93	77.85
	SmA–Iso	134	5.37	13.20
2nd Cooling	SmA–Iso	59	–5.43	–13.22
	SmA–Cr	63	–22.73	–68.41
3rd Heating	Cr^1–Cr^2	86		
	Cr^2–SmA	92	27.50	76.64
	SmA–Iso	134	5.38	13.21
3rd Cooling	SmA–Iso	138	–5.45	–13.25
	Cr–SmA	61	–23.45	–70.21

(a)

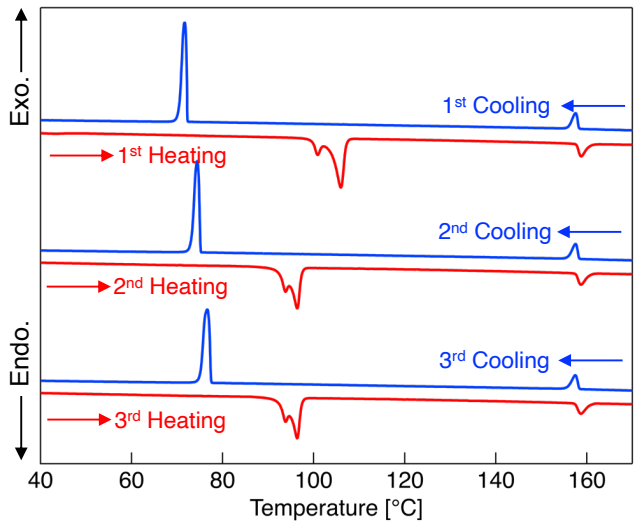

(b)

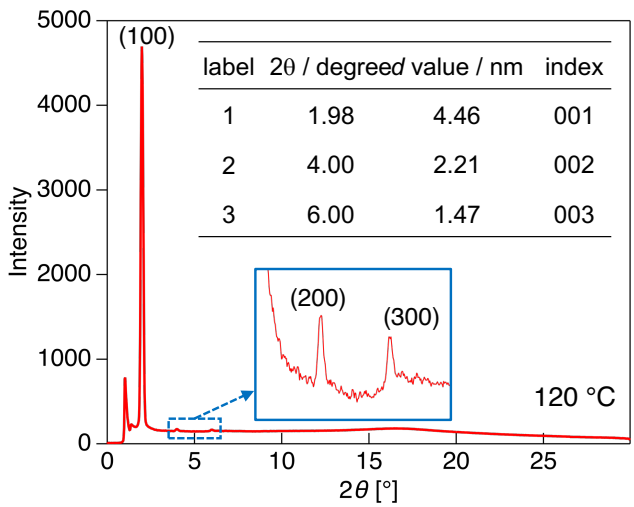

(c)

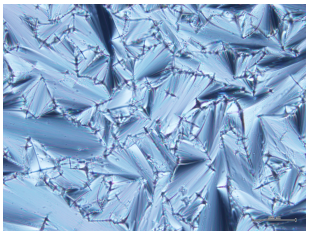

Figure S25. (a) DSC thermograms of **1c** during the heating and cooling processes under N_2 atmosphere. Scan rate: 5.0 °C min^{-1}. (b) Powder X-ray diffraction patterns of **1c** measured at 120 °C in SmA phases. (c) Optical texture image of **1c** at 120 °C during the cooling process.

Table S6. Phase sequence of **1c** and the phase-transition enthalpy and entropy

1c	Phase sequence	Phase transition temperature [°C]	ΔH [kJ mol^{-1}]	ΔS [J mol^{-1} K^{-1}]
1st Heating	Cr^1–Cr^2	100		
	Cr^2–SmA	106	41.67	111.82
	SmA–Iso	158	5.90	13.71
1st Cooling	SmA–Iso	158	–5.74	–13.31
	Cr–SmA	72	–28.06	–81.27
2nd Heating	Cr^1–Cr^2	92		
	Cr^2–SmA	96	30.80	84.29
	SmA–Iso	157	5.75	13.35
2nd Cooling	SmA–Iso	158	–5.68	–13.16
	Cr–SmA	75	–28.04	–80.53
3rd Heating	Cr^1–Cr^2	92		
	Cr^2–SmA	96	30.49	83.45
	SmA–Iso	157	5.64	13.11
3rd Cooling	SmA–Iso	158	–5.64	–13.10
	Cr–SmA	77	–28.28	–80.67

Photophysical behavior

The UV-vis absorption spectra were recorded using a JASCO V-750 absorption spectrometer. The PL spectra of the solution and crystalline forms were acquired using a JASCO FP-6600 fluorescence spectrometer or a Hamamatsu Photonics Quantaurus-QY. The absolute quantum yields in both the solution and crystalline phases were measured using the Quantaurus-QY C11347-01 absolute PL quantum yield spectrometer (Hamamatsu Photonics). The solution sample was prepared by dissolution in CH_2Cl_2 and the concentration was adjusted to 1.0×10^{-5} mol L^{-1} for absorption measurements or 1.0×10^{-6} mol L^{-1} for PL measurements. The crystalline sample was prepared by recrystallization from a CH_2Cl_2/methanol (*v/v* = 1/1) mixed solvent system. The LC phase molecular aggregate sample was prepared by freezing the LC sample using liquid nitrogen immediately after the phase transition.

(a) Hexane (λ_{ex} = 300 nm)

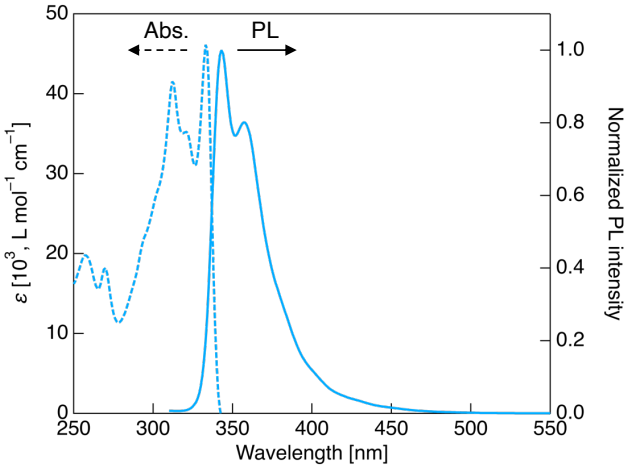

(b) CH_2Cl_2 (λ_{ex} = 321 nm)

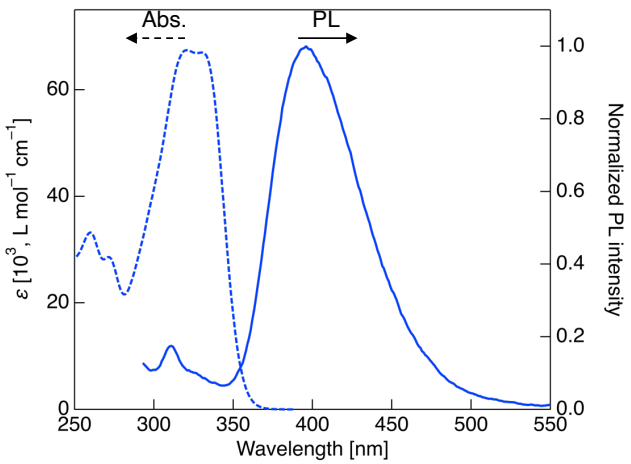

(c) THF (λ_{ex} = 318 nm)

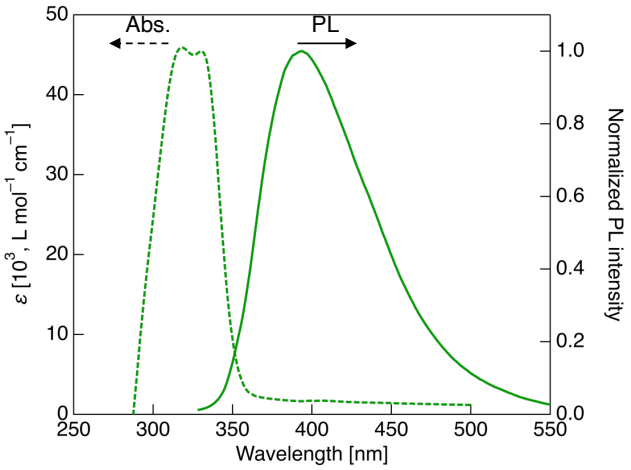

(d) EtOAc (λ_{ex} = 272 nm)

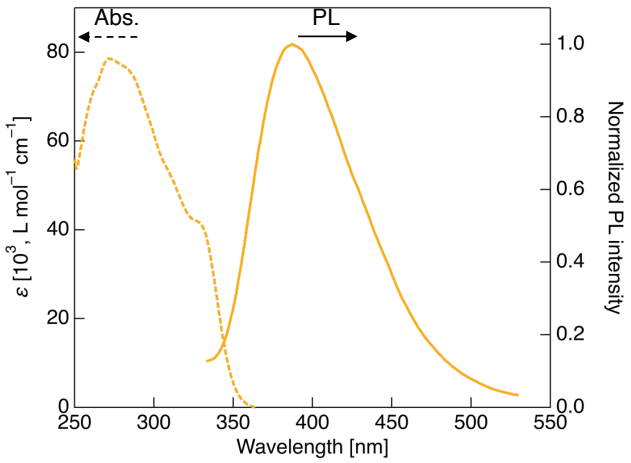

(f) MeCN (λ_{ex} = 331 nm)

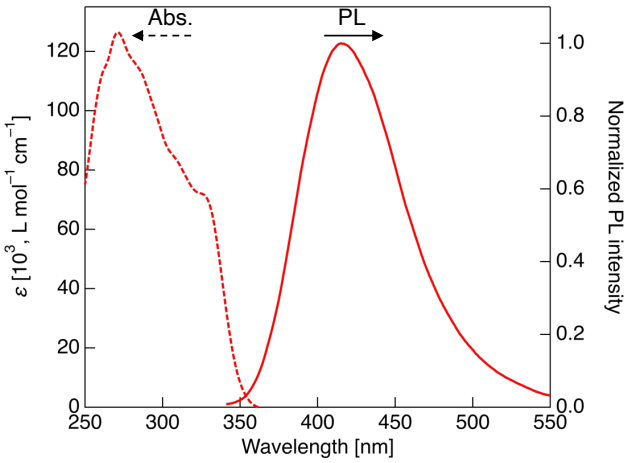

Figure S26. UV-vis and PL spectra of **1a** in various solvent.

Table S7. Photophysical data in various solvent

	ε	ν	Δf	ν_{Abs} [cm^{-1}]	ν_{PL} [cm^{-1}]	$\Delta\nu$ [cm^{-1}]
hexane	1.88	1.37	0.00041099	30030	29155	875
EtOAc	6.02	1.37	0.20050637	30675	25840	4835
THF	7.58	1.4	0.21205627	30303	25445	4858
DCM	8.93	1.42	0.21851142	30303	25253	5050
MeCN	35.9	1.34	0.30610758	30675	24096	6579

Solvent polarity parameter: $\Delta f = \frac{\varepsilon-1}{2\varepsilon+1} - \frac{n^2-1}{2n^2+1}$

Lippert-Mataga equation: $\Delta\nu = \nu_{abs} - \nu_{PL} = \frac{2(\mu_e-\mu_g)^2}{hca^3}\Delta f + constant$

(a) (b)

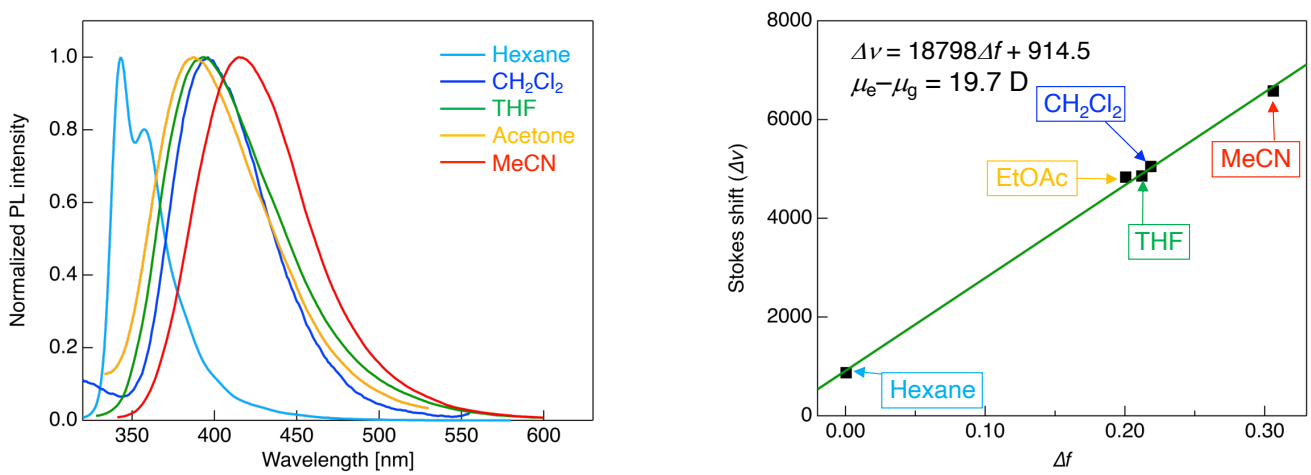

Figure S27. (a) PL spectra of **1a** in various solvent. (b) Lippert-Mataga plot for **1a**.

(a) Hexane (λ_{ex} = 300 nm)

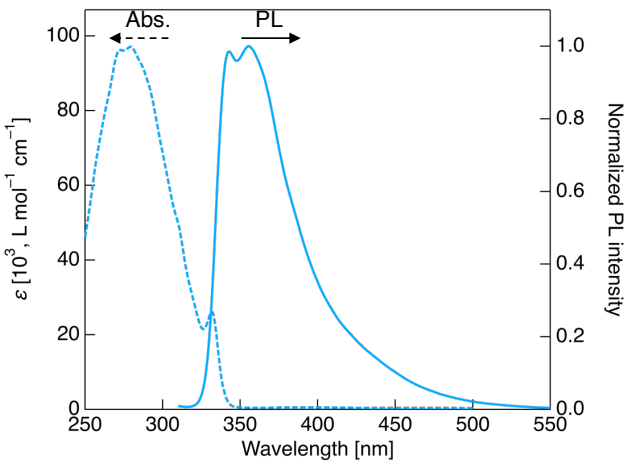

(b) CH_2Cl_2 (λ_{ex} = 321 nm)

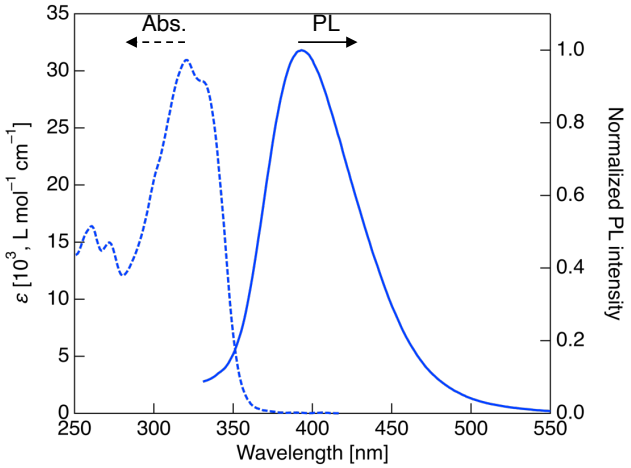

(c) THF (λ_{ex} = 333 nm)

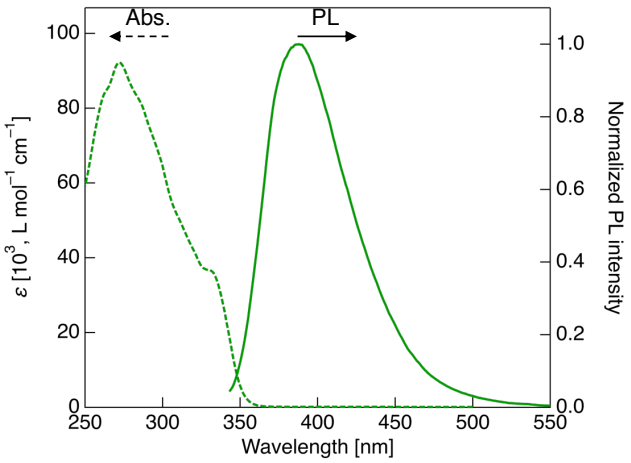

(d) EtOAc (λ_{ex} = 270 nm)

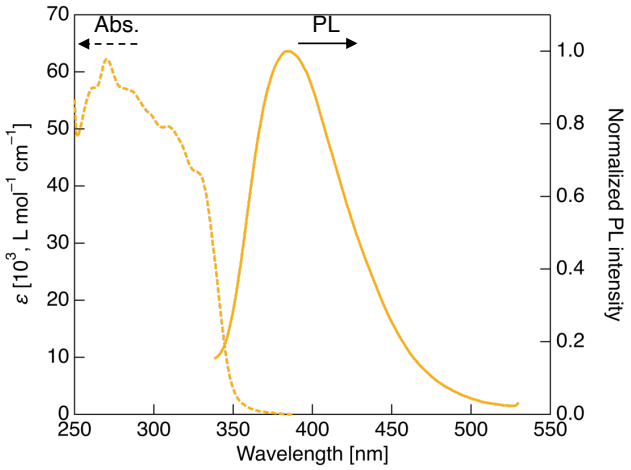

(f) MeCN (λ_{ex} = 334 nm)

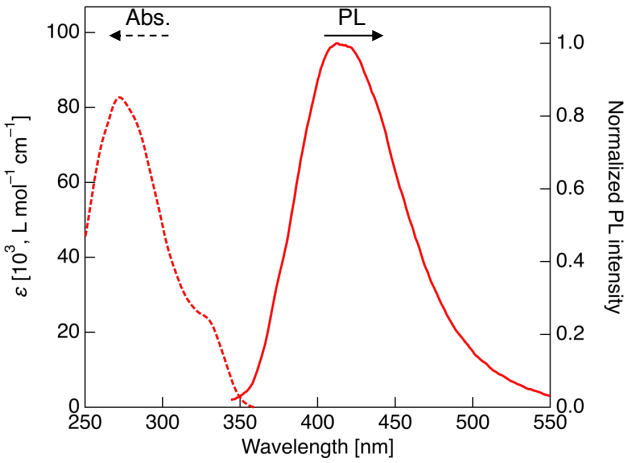

Figure S28. UV-vis and PL spectra of **1b** in various solvent.

Table S8. Photophysical data in various solvent

	ε	ν	Δf	ν_{Abs} [cm^{-1}]	ν_{PL} [cm^{-1}]	$\Delta\nu$ [cm^{-1}]
hexane	1.88	1.37	0.00041099	30120	29155	965
EtOAc	6.02	1.37	0.20050637	30488	26042	4446
THF	7.58	1.4	0.21205627	30303	25773	4530
DCM	8.93	1.42	0.21851142	30303	25381	4922
MeCN	35.9	1.34	0.30610758	30675	24213	6462

Solvent polarity parameter: $\Delta f = \frac{\varepsilon-1}{2\varepsilon+1} - \frac{n^2-1}{2n^2+1}$

Lippert-Mataga equation: $\Delta\nu = \nu_{abs} - \nu_{PL} = \frac{2(\mu_e-\mu_g)^2}{hca^3}\Delta f + constant$

(a) (b)

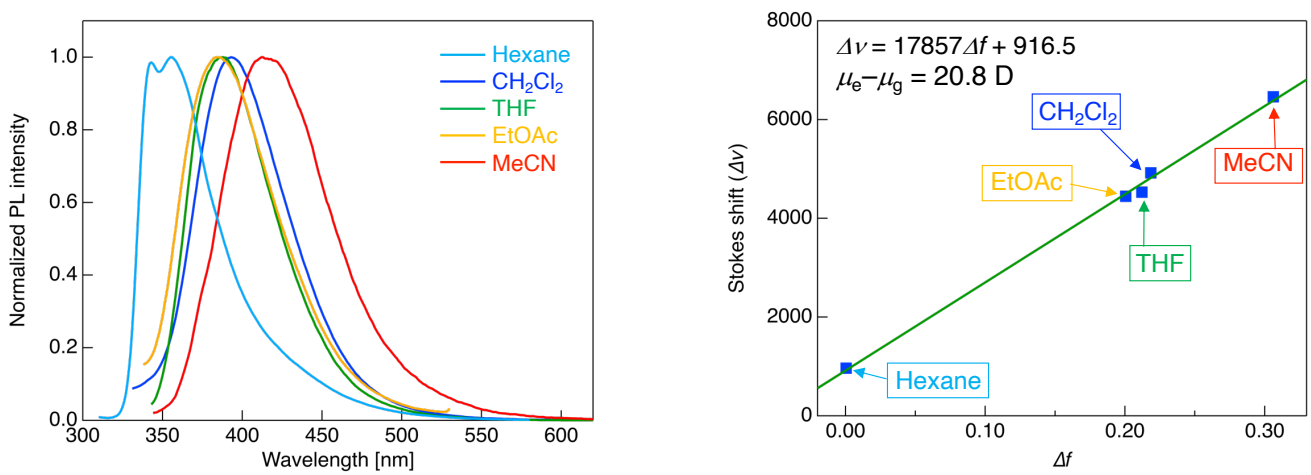

Figure S29. (a) PL spectra of **1b** in various solvent. (b) Lippert-Mataga plot for **1b**.

(a) Hexane (λ_{ex} = 271 nm)

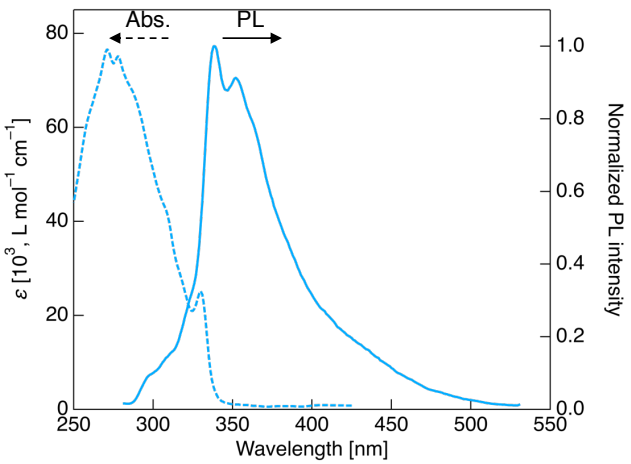

(b) CH_2Cl_2 (λ_{ex} = 321 nm)

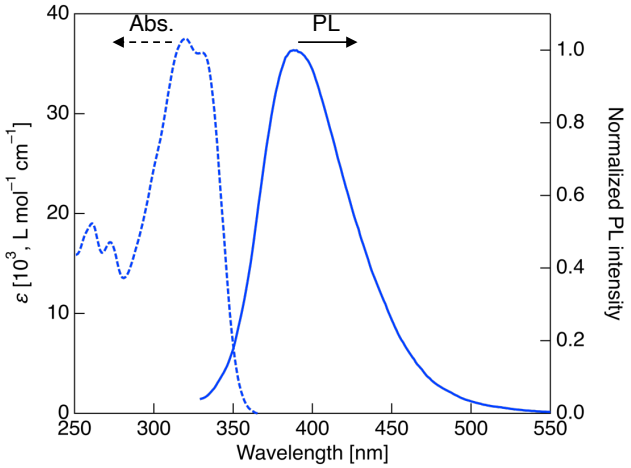

(c) THF (λ_{ex} = 317 nm)

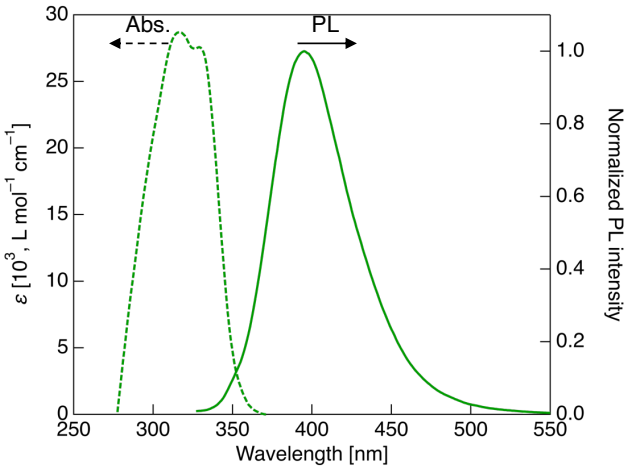

(d) EtOAc (λ_{ex} = 310 nm)

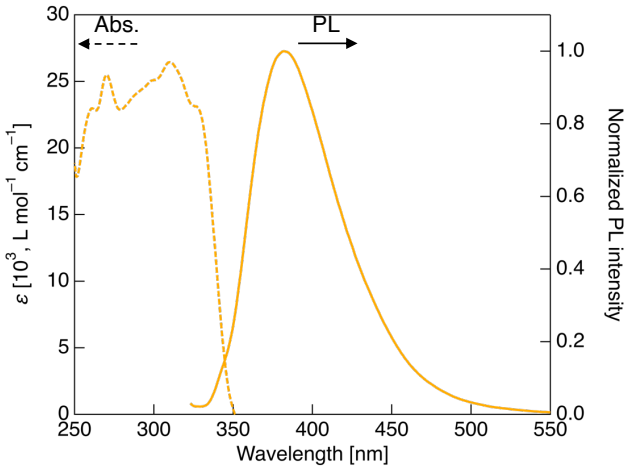

(f) MeCN (λ_{ex} = 271 nm)

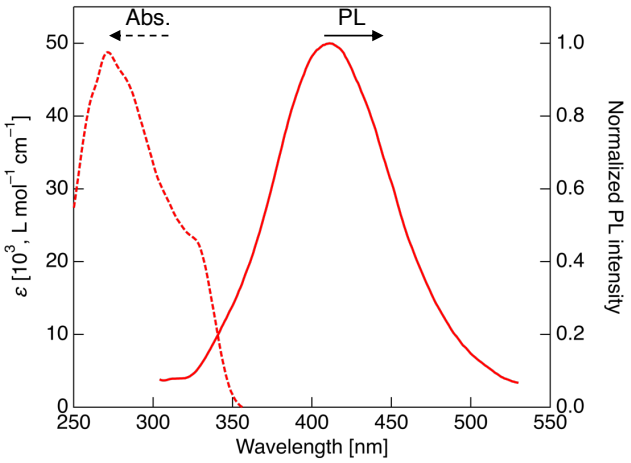

Figure S30. UV-vis and PL spectra of **1c** in various solvent.

Table S9. Photophysical data in various solvent

	ε	ν	Δf	ν_{Abs} [cm^{-1}]	ν_{PL} [cm^{-1}]	$\Delta\nu$ [cm^{-1}]
hexane	1.88	1.37	0.00041099	30303	29586	717
EtOAc	6.02	1.37	0.20050637	30581	26178	4403
THF	7.58	1.4	0.21205627	30303	25316	4987
DCM	8.93	1.42	0.21851142	30211	25773	4438
MeCN	35.9	1.34	0.30610758	30769	24331	6438

Solvent polarity parameter: $\Delta f = \frac{\varepsilon-1}{2\varepsilon+1} - \frac{n^2-1}{2n^2+1}$

Lippert-Mataga equation: $\Delta\nu = \nu_{abs} - \nu_{PL} = \frac{2(\mu_e-\mu_g)^2}{hca^3}\Delta f + constant$

(a) (b)

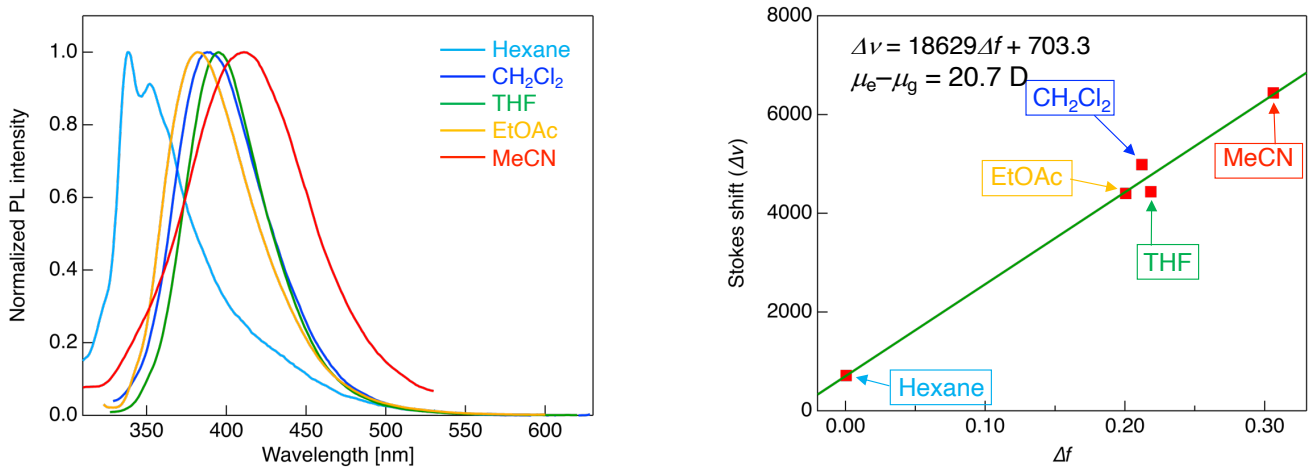

Figure S31. (a) PL spectra of **1c** in various solvent. (b) Lippert-Mataga plot for **1c**.

(a)

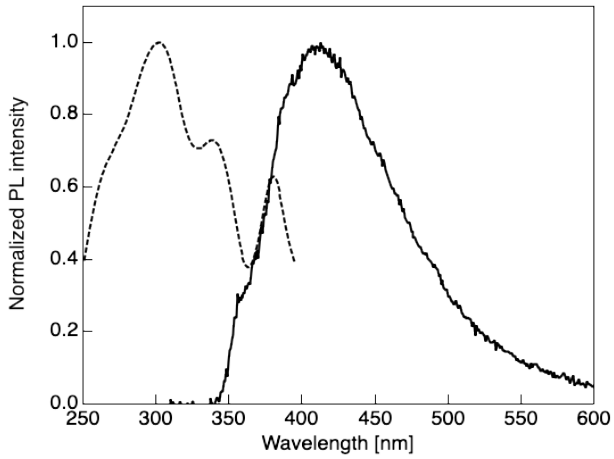

(b)

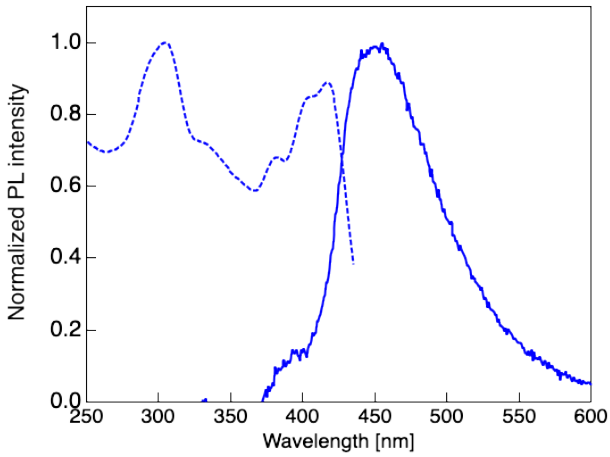

(c)

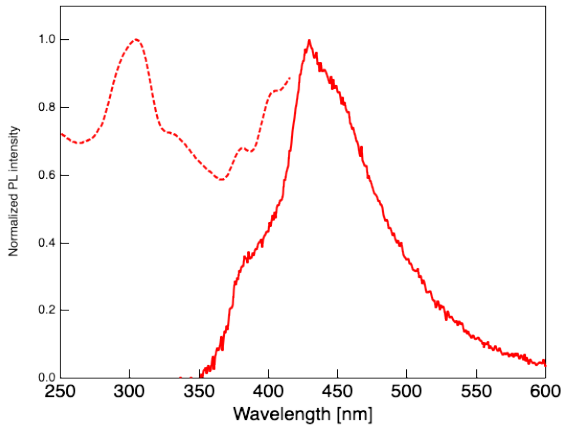

Figure S32. Excitation and PL spectra of (a) **1a**, (b) **1b**, and (c) **1c** in crystalline phase. Excitation wavelength (λ_{ex}) = 300 nm for **1a**–**c**. Excitation spectra were obtained by using the Quantaurus-QY with a Excitation-wavelength scan method. Monitoring wavelength region: 403–425 nm for **1a**, 445–465 nm for **1b**, and 420–440 nm for **1c**.

Powder X-ray diffraction

Powder X-ray diffraction patterns were measured using an X-ray diffractometer (Rigaku MiniFlex600) equipped with an X-ray tube (CuKα, λ = 1.54 Å) and semiconductor detector (D/teX Ultra2). The sample powder was mounted on a silicon non-reflecting plate, and the plate was set on a benchtop heating stage (Anton Paar, BTS-500).

(a) **1a**

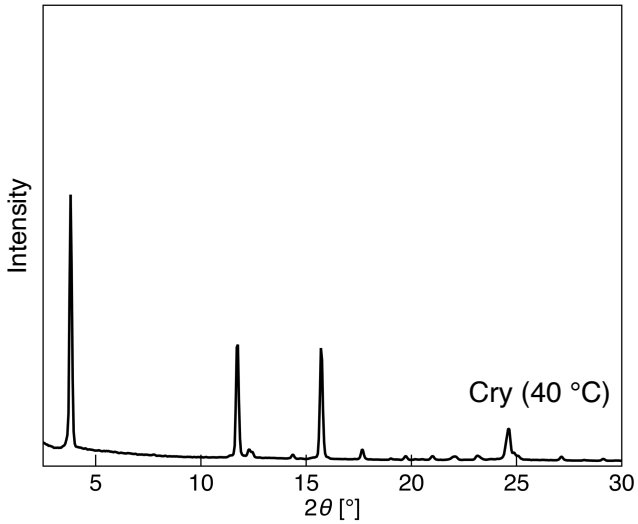

(b) **1b**

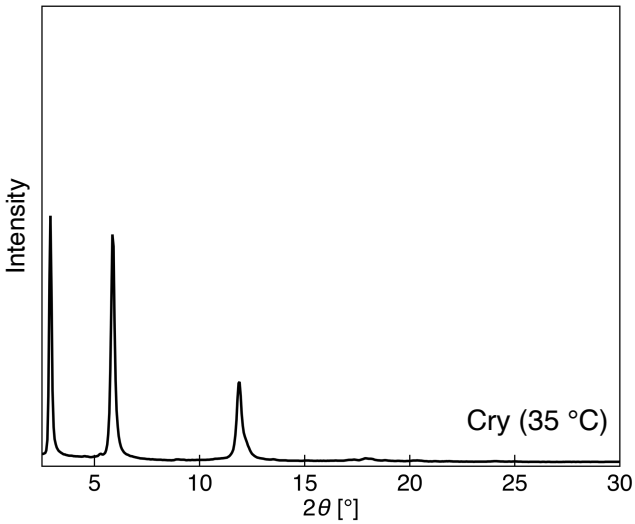

(c) **1c**

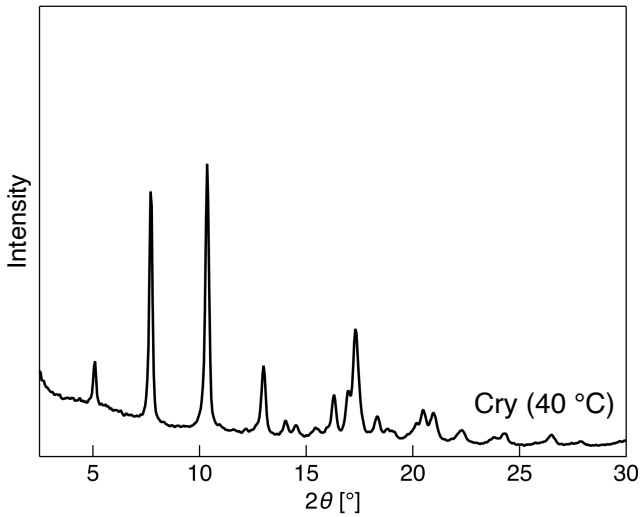

Figure S33. Powder X-ray diffraction of (a) **1a**, (b) **1b**, and (c) **1c** at room temperature.

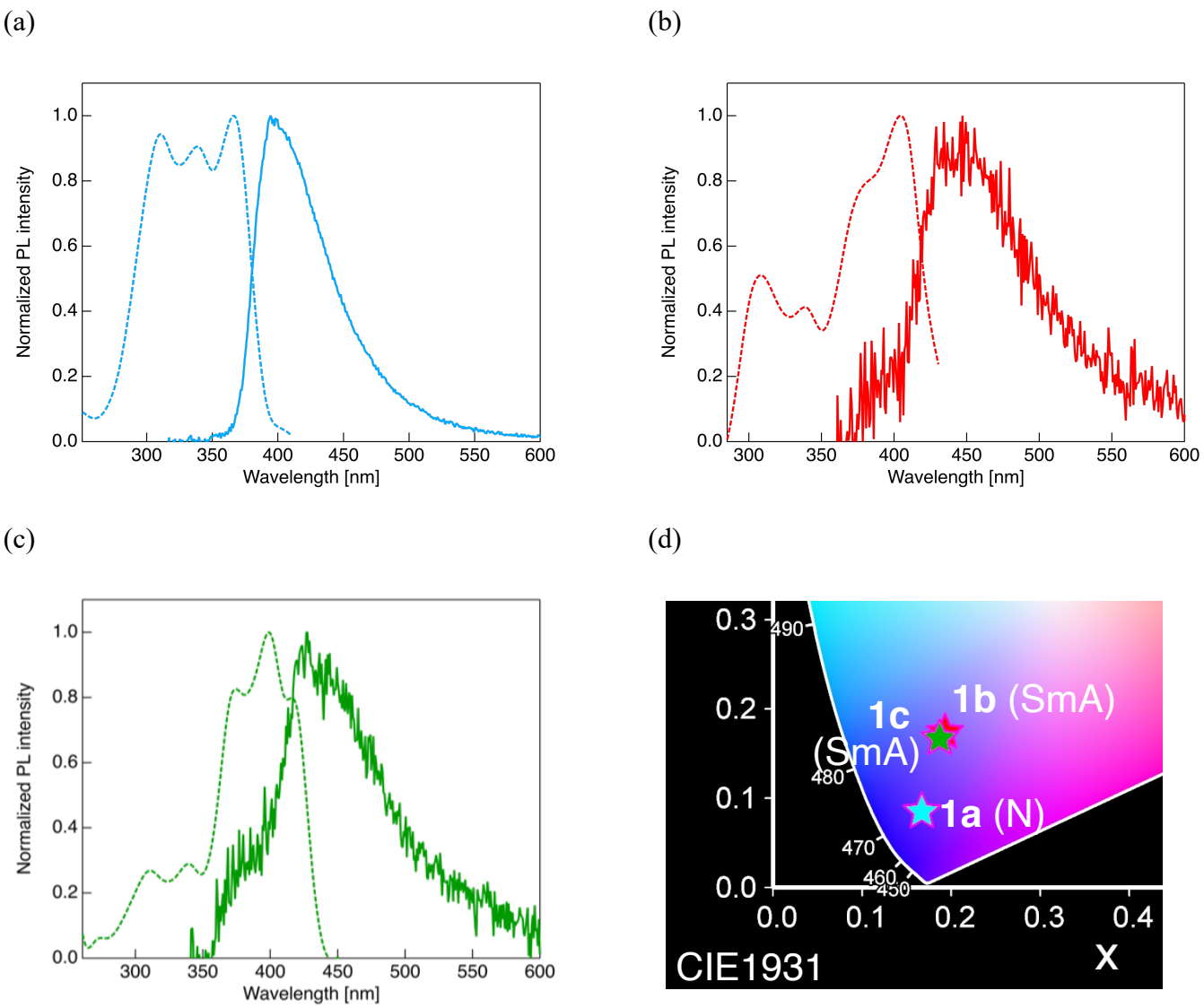

Figure S34. (a) Excitation and PL spectra of **1a** in N phase structure, (b) **1b** in SmA phase structure, and (c) **1c** in SmA phase structure. Excitation wavelength (λ_{ex}) = 300 nm for **1a** and 340 nm for **1b** and **1c**. Excitation spectra were obtained by using the Quantaurus-QY with a Excitation-wavelength scan method. (d) CIE plot for PL color of **1a**, **1b** and **1c** in the LC phase structure.

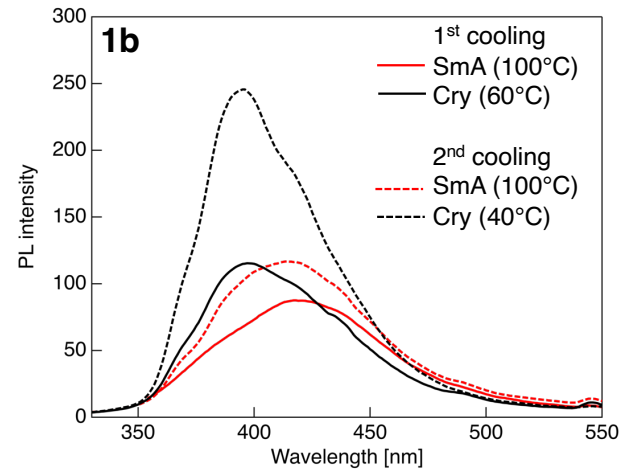

Figure S35. PL spectra of **1b** under 1st and 2nd cooling process using fluorescence spectrometer.